



TECHNISCHE
UNIVERSITÄT
WIEN

MASTER THESIS

Characterization of electrical biosensors to monitor placenta barrier integrity

Submitted at the

Institute of Technical Chemistry,

Vienna University of Technology

under supervision of

Univ. Prof. Dipl. -Ing. Dr. Peter Ertl,

Dr. Mario Rothbauer

by

Hajnalka Gondola

Matr.Nr. 1427465

Wien, May 2017

*To my best friend
Rest in peace, dear T*

Acknowledge

First of all, I would like to express my gratitude to Peter Ertl, for the opportunity to join CellChip Group and make this thesis possible. My sincere thanks go to Mario Rothbauer for his support during my work, for his patience, motivation, and immense knowledge. I also thank the colleagues of whole group for their help.

Special thanks go to my family and friends, for their support during my studies and in my life general.

Contents

1. Introduction	5
2. The Placenta	7
2.1. Placental Blood Circulation.....	7
2.2. The placental barrier	9
2.2.1. Placental transfer	10
2.3. Models of the placenta	10
2.3.1. <i>Ex vivo</i> models	11
2.3.2. Animal models.....	11
2.3.3. <i>In vitro</i> models.....	12
3. Lab-on-a-chip systems - new generation model for life science research	12
3.1. Cell-based microfluidics.....	12
3.2. Biosensors.....	14
3.2.1. Piezoelectric biosensors	15
3.2.3. Electrochemical biosensors	16
4. Organ-on-a-chip devices.....	18
4.1. Placenta-on-a-chip - an expanding microdevice.....	19
4.2. Transepithelial/endothelial electrical resistance measurements (TEER)	21
5. Theoretical Background.....	22
5.1. Impedance of cells.....	22
5.2. Transepithelial/endothelial electrical resistance measurement according to Ohm's law	24
5.2.1. Electrode configuration for transepithelial/endothelial electrical resistance measurement.....	26
5.3. Impedance spectroscopy	26
5.3.1. Two- and four electrode impedance measurement setup	27
6. Materials and Methods	28
6.1. Cell culture basics	28
6.1.1. Cultivation of placenta cells	28
6.1.2. Cell counting method.....	29
6.1.3. Cell characterization	29
6.2. Viability test	30
6.3. Transepithelial/endothelial electrical resistance measurements	32
6.3.1. Characterization of the measurement method.....	32
6.4. Chip design considerations for impedance spectroscopy	33

6.4.1.	Blank chip for monitoring cell morphology.....	33
6.4.2.	Characterization of PDMS bonding.....	34
6.4.3.	Coplanar chip for impedance measurement.....	34
6.4.4.	Final coplanar electrode design.....	35
6.5.	Placenta station for cell adhesion measurement.....	36
6.6.	Placenta barrier integrity measurement	37
6.6.1.	Measurement characterization	37
6.6.2.	Cytotoxicity test of ATCC and B30 cell-lines.....	37
7.	Results.....	38
7.1.	Characterization of cell morphology.....	38
7.2.	Cytotoxicity test on placenta cell lines.....	39
7.2.1.	Cytotoxicity test of colchicines, chlorpromazine and MMS.....	39
7.2.2.	Cytotoxicity measurements of SiO ₂ nanoparticles.....	44
7.3.	Trans-epithelial endothelial resistance measurements	46
7.3.1.	Characterization of TEER.....	47
7.3.2.	TEER experiment with different seeding density	48
7.3.2.	TEER permeability experiment.....	50
7.3.3.	TEER permeability experiment on SiO ₂ nanoparticle	52
7.4.	Electrical impedance spectroscopy measurements.....	54
7.4.1.	Electrode characterization for electrical cell-substrate impedance sensing	54
7.4.2.	Characterization of EIS measurement with physiological buffer	57
7.4.3.	Impedance spectroscopy measurement to monitor cell adhesion.....	58
7.4.4.	Toxicity measurement of ATCC and B30 cells during impedance spectroscopy.....	59
8.	Summary and Outlook	62
9.	References.....	63
10.	List of figures	65

1. Introduction

Environmental exposures during pregnancy have gained more attention in recent decades, not only for women but also for health care providers. The importance of drug control distribution has been established, since substances delivered to the mother can possibly penetrate the placental barrier. But the process to reorder the priority in favor of the safety of mother and fetus has not been considered necessary. Even though up to 85% of pregnant women need to take medication, only every third drug has been tested for fetal safety [1]. However, in some cases taking medicaments during pregnancy is inevitable, with the leading acute/short-term illness being headache, fever, pain and nausea and the chronic/long-term illness being hypothyroidism, asthma, allergy and depression [2]. For instance a prominent example is thalidomide, which was widely used to treat nausea of pregnant women [3]. However, the drug resulted in severe birth defects. Due to the media attention back then, this can be considered as turning point in the awareness for drug-induced toxicity, thus the starting point for toxicity testing. More recently, Zika virus has been discovered in South America, resulting in severe brain malfunction in the newborn. Additionally, a survey conducted by Brent et al. has provided that exposure to medications, alcohol, or other factors can result in congenital anomalies for 1 in 10 pregnancies [4]. Furthermore, harmful mother drug intake can end up in preterm birth, fetal growth restriction, or developmental disabilities such as behavioral, neurological, motor or intellectual defects. In the most extreme cases spontaneous abortion, late fetal death and neonatal death can be accounted also caused by harmful drugs [5].

Because of the above mentioned issues it is crucial to investigate the permeability of the placenta barrier towards bioactive substances. Since the *in vivo* experiments on humans are limited due to ethical reasons, different alternative models were established including *in vivo* animal models, *ex vivo* placental perfusion systems and *in vitro* cell cultures. These models are able to mimic the human-relevant physiology accurately, but researchers still cope with difficulties such as lack of standardization due to lab-to-lab variations. For instance most primary tissue samples applied for *ex vivo* models are mainly 7-9 months old and therefore

cannot resemble early stages of pregnancy. Due to ethical concerns as well as high costs of animal models, animal in vivo studies also do not provide the best solution.

To overcome these existing limitations, in this thesis the development of a microengineered biomimetic model for placenta drug screening is presented. Such models have already been developed to simulate the structure and function of the placenta in order to gain a better understanding of this complex organ [6].

The aim of the thesis is to investigate the effect of different substances and silica nanoparticle on different placenta cells. Here, microfluidic technology in combination with electrochemical biosensors will be established and characterized to create a placenta-on-a-chip that is capable of non-invasive monitoring of drug induced toxicity. Further the system will be tested against state of the art techniques employing placental transwell cultures and transepithelial electrical resistance measurements (TEER).

2. The Placenta

The placenta is a unique, complex organ with the primary function of surrogating respiration, excretion and digestion in order to support the normal growth and development of the fetus [7]. It forms the interface between the maternal and fetal circulation, maintains the exchange of nutrients and also the fetal waste disposal. Furthermore, the placenta releases hormones to adjust maternal physiology during pregnancy and acts as a barrier against the maternal immune system [8].

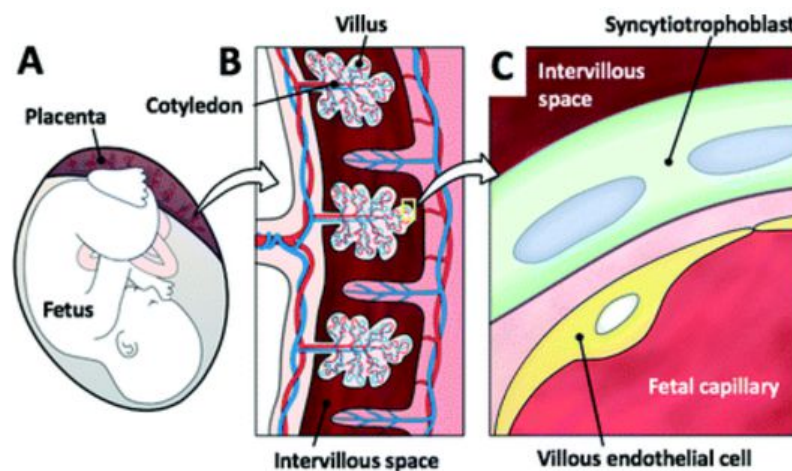


Figure 1.: A. Schematic model of a human placenta and fetus. B. Cross-sectional view of the placenta illustrates the placental cotyledons. Each cotyledon consists of a stem chorionic villus and its branches. C. The maternal intervillous space is separated from the lumen of the fetal capillary by the maternal-fetal interface composed of the syncytiotrophoblast, basal lamina, and villous endothelial cells.

In humans a healthy and fully developed placenta consists of three different layers: the outer maternal layer with decidual cells of the uterus and the maternal vasculature for blood supply with the implantation site. The middle „junctional” region consists of fetoplacental trophoblast cells and connects the fetal placenta to the uterus. These cells line the wall of uterine and maternal vessels [9]. Finally, the inner layer is built by complex branches of villi responsible for nutrient exchange [10].

2.1. Placental Blood Circulation

Placenta has two separate circulation systems for blood supply: uteroplacental (maternal-placental) and fetoplacental (fetal-placental) blood circulation. The uteroplacental blood circulation is responsible mainly for the exchange of blood and nutrients. The blood flows

into the intervillous space through decidual spiral arteries. The deoxygenated blood is pushed back to the maternal circulation via endometrial and then uterine veins. During the pregnancy, the flow of the placental blood is increased; its volume can reach up to 600-700 ml/min. The highest blood pressure can be obtained in the uterine arteries about 80-100 mmHg, in spiral arteries 70 mmHg and the lowest is within the intervillous space, only 10 mmHg. Due to the low-resistance of the uteroplacental vessels and the gradient of the blood pressure between uterine arteries and placental intervillous space the blood in the intervillous space is fully exchanged in every 20-30 seconds. In fetoplacental circulation the deoxygenated and nutrient-depleted fetal blood is introduced to the villous core fetal vessels by the umbilical arteries. After the exchange, the fresh blood enters the fetal systemic circulation. The value of the blood pressure falls from 50 mmHg to 30 mmHg in the umbilical arteries when the blood flows to the capillaries in the villi. The vein pressure of the umbilical is 20 mmHg. The fetal vessels are protected against collapse by the blood pressure of the fetal vessels, as their villous branches is constantly higher than that within the intervillous space [11].



Figure 2.: Blood circulation of the placenta, showing the directions of blood flow from mother to the placenta and fetal blood flow from the placenta to fetus.

Information about the health can be obtained by measuring the volume of the forward blood flow through the umbilical artery during both systole and diastole, since there is a linear relationship between the health of the fetus and the amount of the forward blood flow.

2.2. The placental barrier

The fetus-maternal circulation is established at the end of the first trimester. The placenta develops into a permeable interface, which is responsible for the regulation of the exchange of nutrients and metabolites [12]. The barrier includes trophoblast cells and small amount of endothelium of fetal capillaries. It has a multilayer structure including endothelial cells, cytotrophoblast cells, basal membrane and syncytiotrophoblasts in the first trimester [13]. The mature placenta, on the other hand, is composed of endothelial cells, structure including endothelial cells, syncytiotrophoblasts and the basal membrane. As a part of the cytotrophoblast layer disappears during the progress of the pregnancy, the membrane becomes more permeable and the trans-placental diffusion distance decreases. Syncytial microvillous (maternal side) and basal membrane (fetal side) will coordinate the transport across the placenta. Transplacental transport is regulated by passive and facilitated diffusion, active transport and pinocytosis across the placental membrane.

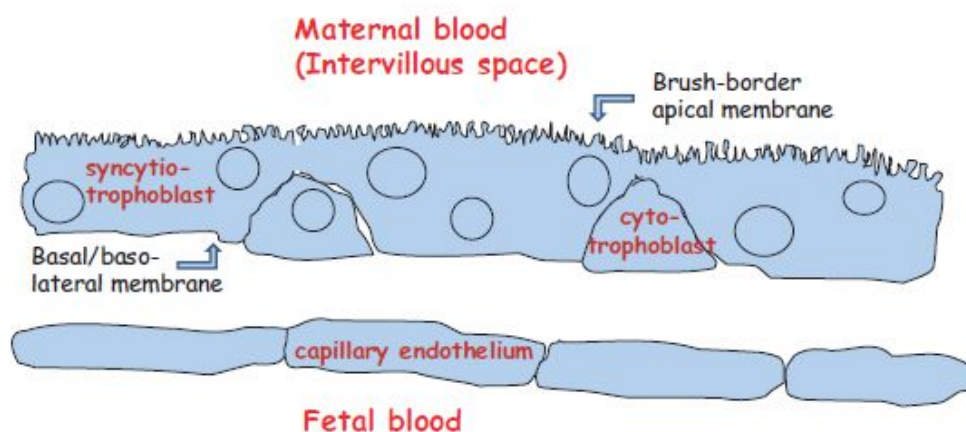


Figure 3.: Schematic representation of the human placental barrier. The placental barrier cells develop thousands of microvilli exposed to the maternal blood in the intervillous space and regulate material transfer between the maternal and fetal blood flow.

2.2.1. Placental transfer

Continuous gas exchange and nutrient supply from maternal blood is required for the normal growth and development of the placenta. This process comprises uptake from the blood of the mother transferred first across the syncytiotrophoblast and cytotrophoblast layers, the underlying basal lamina, the fetal connective tissue space, and the fetal capillary endothelium [14]. The placental membrane is highly permeable to respiratory gases, but it is still less efficient than the lung. The transport between gases occurs rapidly, and is mediated by diffusion. The blood of the fetus has a higher hemoglobin concentration, greater affinity for oxygen [13]. The primary fuel for the fetal is provided by glucose, derived from the maternal plasma, as an essential component of the fetal oxygen consumption [14]. The transfer is mediated by facilitated diffusion, involved with membrane carrier. The rate of the diffusion can be raised by combining the membrane carrier with glucose. This mixing results in higher solubility of glucose in the lipid bilayer portion of the membrane [15]. Fructose and lactate are also found in the plasma in smaller quantities. Fructose is synthesized from D-glucose, lactate is produced by D-glucose. For both of them the placenta membrane is almost impermeable. Amino acids are transported across the placenta via active transport mediated by the microvillous and the basal membranes with the help of specific transporters [16]. They play an important role in protein synthesis and can be processed by the fetus. Fat-soluble vitamins are transported by simple diffusion, while they are bound to proteins [15].

2.3. Models of the placenta

The placenta maintains the fetus during the pregnancy and is responsible for the normal growth of the embryo. However, the knowledge about placental structure and its function is strictly limited due to ethical reasons and availability of primary tissue and organ samples. With the help of different models that were established and developed throughout the years, better understanding can of placental physiology and malfunction can be achieved, including *ex vivo* models, animal models as well as *in vitro* models.

2.3.1. Ex vivo models

The *ex vivo* placental perfusion model is widely used to monitor placental transport of different compounds across the maternal-fetal barrier without ethical barriers. Non-invasive experiments can be carried out and it is able to represent the *in vivo* situation in humans on the highest accuracy. However, one of the most striking disadvantages of this model is the limited number of experiments as well as the short viability of the organ samples. The placentas used for the measurements are donated from the mothers after delivery and are mostly 7 to 9 months old. Therefore these samples fail to represent transport in the first and second trimester of the gestation [17]. These models are not only technically challenging and very labor consuming but the maternal vasculature of the placenta is damaged during separation and delivery. In order to overcome the issue, laboratories established different protocols for cannulation and perfusion of the maternal side without standard criteria, thus their results cannot be compared [18]. The tissue preparation models were useful for the examination of the variety of chemicals and medications by the placental tissue and the uptake of transporters. The models were based on placental tissue explants and plasma membrane vesicles. With the help of these models cell-cell interactions and transporter functions could be monitored, but they are not able to mimic *in vivo* conditions and the STC may be damaged during the process [19].

2.3.2. Animal models

Animal experiments are used first of all for *in situ* studies [20]. Depending on what mechanism and functions are investigated, different animals are used, such as guinea pig, rat, and rodents. For instance placental transfer and fetal growth restriction is studied using via guinea pig model. Sheeps are used examining the placental vascular development and nutrient exchange. Rodents are most commonly used in animal experiments. They are favored for easy housing conditions, short gestational length and are economically affordable [21].

2.3.3. *In vitro* models

To overcome the drawbacks of *ex vivo* models such as lack of early stages of placenta cells furthermore the costs and ethical concerns of animal models wide range of cell cultures models were also developed over the years in order to observe the transport and metabolism. The primary placental cells can be investigated at any stage of gestation and the cell line- that was also in use for this model- is replicated rapidly in culture. The model of trophoblast-like cell lines (e.g. JAR, JEG-3, BeWo) are widely used for transport studies. The co-cultured monolayer gives an insight into the transport of several substances line nutrients, amino acids, folic acids. [22], [23], [24]. The disadvantages of these models are that there is a high contamination level and normal STC cannot be mimicked.

3. Lab-on-a-chip systems - new generation model for life science research

Due to the limitations of the above mentioned models, it is inevitable to find new, reliable and ethical solutions to examine, monitor different organs in the human body *in vitro*. This section gives a brief summary about the most important inventions in the field of cell-based microfluidics, biosensors, which in the near future will take over a significant part of the *in vivo* experiments [25].

3.1. Cell-based microfluidics

In the last decades, the basic techniques of microfluidics for the study of cells such as cell culture, cell separation, and cell lysis, has been well developed. Cell-based microfluidics gives a new approach in drug discovery and delivery such as in clinical diagnostics, genetics research, bio-weapons detection, and immunology. This has resulted that miniaturized components and processes, decreasing costs and permitting small quantities of precious samples are stretched further. Furthermore, smaller volumes of liquid, less reagent consumption is required. This leads to reduced quantities of waste products [26]. Accuracy and efficiency of detection is improved by the small scale of microfluidic devices, where the

length of the channels becomes comparable to the size of the materials to be analyzed. Shortened measurement times, higher sensitivity can be also obtained. The process parameters in chemical reactions are better controllable, thus a cell analysis runs faster and its results are delivered even within a few seconds.

The advantages offered by microfluidic devices over traditional instruments for chemical and biological analysis are the reasons why microfluidics is considered one of many highly advanced technologies that are able to revolutionize our everyday life in the near future. In the next section, different cell-based applications will be discussed briefly, developed by research groups.

Barker and Lu et al. have come up with a new and promising design of microfluidic chip with a 2*4 addressable array chamber. The architecture of the array enables continuous perfusion through each chamber, no cross-chamber communication, and chamber shielding in order to decrease shear stress introduced to the cells. Simultaneously, an enormous range of diversity is ensured, as well as experimental parallelization. This type of set of arrangement was tested by studying the epithelial-to-mesenchymal transition (EMT) of alveolar epithelial cells in response to pairwise combinations of immobilized (Ln/Fn) and soluble (TGF- β 1) signals [27].

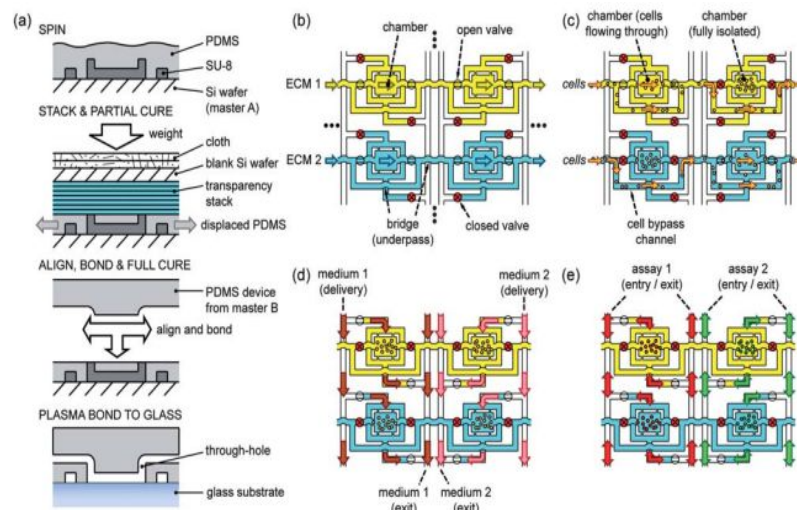


Figure 4.:(a) The fabrication method of the PDMS contains soft lithography, thermal bonding, and compression-molding. (b) ECM incubation: matrix molecules adsorb to chamber surfaces by rows or individual chambers. (c) Cell loading: cell suspension are introduced to rows, while chambers are isolated to limit and regulate cells. (d) Culture: channels are designed to avoid cross-chamber communication: flows over/under other flows. (e) Assay: cells with desired probes are labeled with solution entered the array from the entry or exit channels.

Ye et al. developed a device suitable for cell-based high content screening (HCS) that disposes multiple drug gradient generators and parallel cell culture chambers, for the integration of liquid dilution, diffusion, micro-scale cell culture, stimulation and labeling on a single device. In this work, multiparametric measurement of cellular responses in human liver carcinoma (HepG2) was carried out. The platform was invented for rapid extraction of the highest amount of information from tumor cells in response to several drugs with different concentration, with minimal sample and shorter time, that is required in the field of cancer treatment [28].

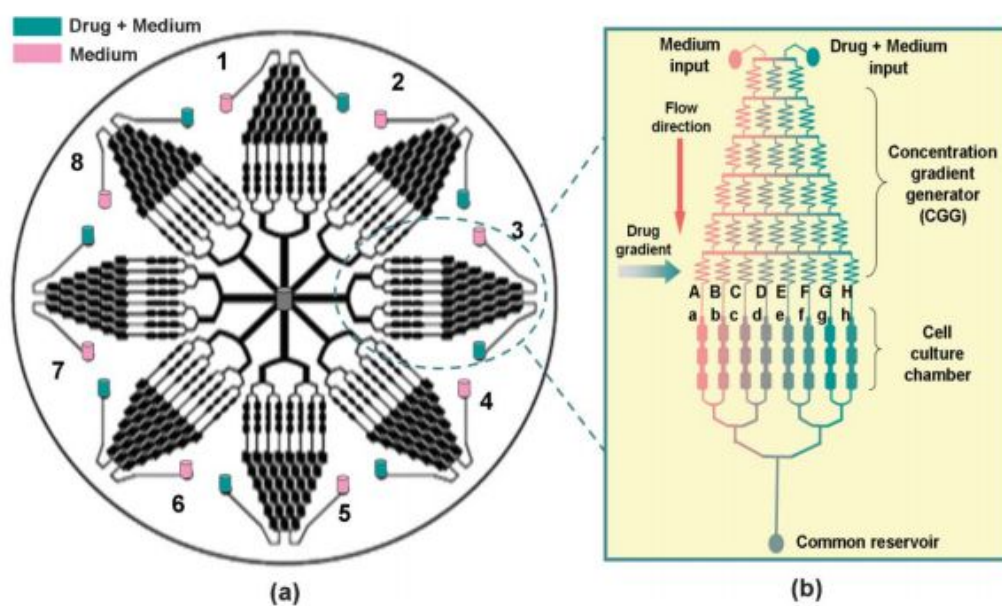


Figure 5.: (a) The device has eight uniform structure units, each of them are connected to the reservoir, placed in the center of the device. (b) Magnifier schematics of the single structure unit with an upstream concentration gradient generator (CGG) and downstream parallel cell culture chambers.

3.2. Biosensors

In a decade, cell-based biosensors have become a research hotspot. The idea is that cell-based biosensors can keep living cells under constant observation to study cellular physiological action when cells are subjected to stimulus [29]. They are capable of detecting and analyzing different forms of cellular responses that occur upon exposure to a broad variety of physical, biological and chemical stimuli (Figure 7.). Biosensors are characterized

by their high sensitivity, excellent selectivity, and rapid response and have been applied in many fields, such as biomedicine, environmental monitoring, and pharmaceutical screening.

Biosensors have been invented in 1962 with the development of enzyme electrodes by Leland C. Clark et al. [30]. Ever since that, various type of biosensors have been developed, such as optical, thermal, piezoelectric, magnetic and electrochemical biosensors, according to their method of signal transduction. In the next section, different cell-based biosensors and their applications will be discussed briefly.

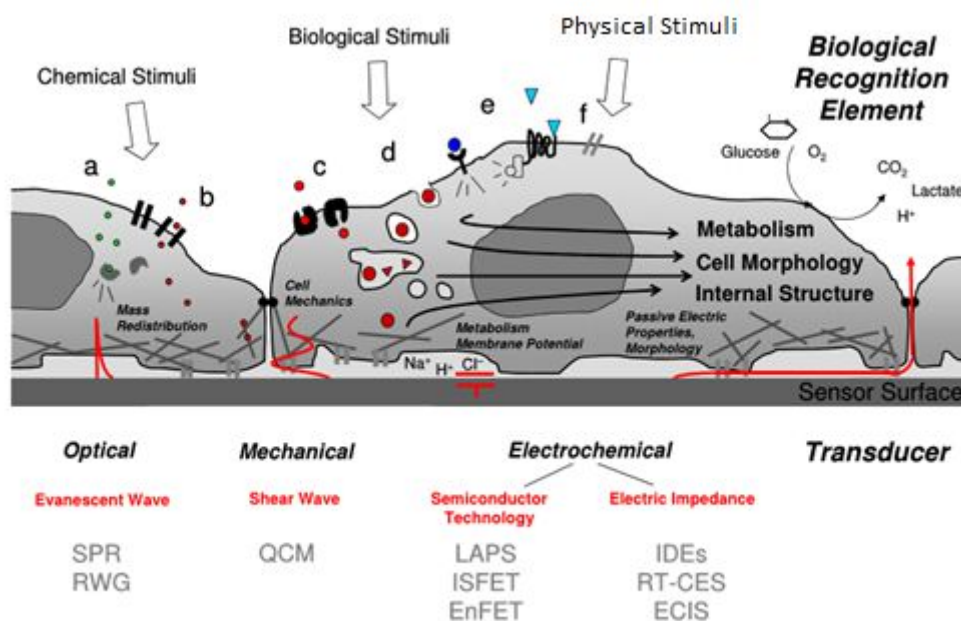


Figure 6.: Brief overview of label-free substrate integrated cell-based biosensors. Different optical, mechanical and electrochemical transducer techniques allow for detection of various forms of cellular responses, like changes in metabolism, internal cell structure and cell morphology.

3.2.1. Piezoelectric biosensors

Piezoelectric biosensors are suitable for assays, where changes of viscosity and surface elasticity are detected such as aggregations, coagulations and precipitations [31]. Quartz crystal microbalance with dissipation monitoring (QCM-D) provides an assessment of changes of a layer of biomolecules attached to the surface of the quartz crystal. With this method, there is the ability to monitor the stepwise development of a biological platform moreover to directly monitor the adsorption of cells on these surfaces [32].

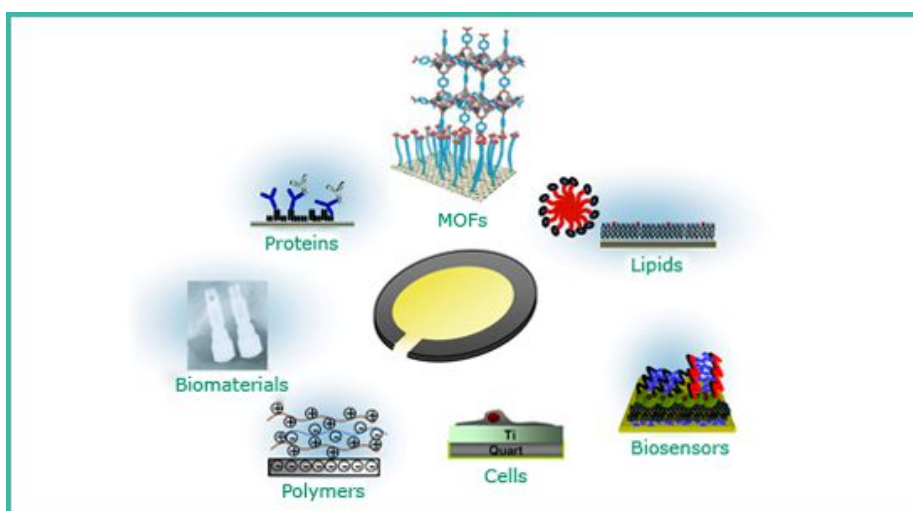


Figure 7.:Quartz crystal microbalance and its applications

3.2.2. Magnetic biosensors

Magnetic biosensors have been proposed as a new means to sensitively detect low concentrations of targets in body fluids for diagnostics [33]. Cartmell et al presented a magnetic force bioreactor in which magnetic nanoparticles were coupled to human osteoblasts and the promotion of the generation of bone matrix was shown by magnetically activated mechanical conditioning [34]. The Ingber group has developed magnetically actuated cellular biochips. These microchips are patterned magnetic arrays which, when activated, promote adhesion of cells (in this case human umbilical vein endothelial cells, HUVECs) bound to magnetic nanoparticles [35]. By utilizing nanomagnetic actuation of specific ion channels and surface receptors on the stem cell membrane, Sura et al, have been able to direct their differentiation completely without the use of chemical agonists [36]. In vitro applications based on magnetic actuation are becoming significant players in the non-viral transfection market, rivalling existing virus-based methods for transporting genes and proteins across cell membranes [37].

3.2.3. Electrochemical biosensors

Electrochemical biosensors have gained attraction in the recent decades- given the increasing demand for practical and low-cost analytical techniques- for use in medicines, quality analysis of drugs. Furthermore, it is interesting for other analytes of interest in the

pharmaceutical area, where for example they allow the analysis of degradation products and metabolites in biological fluids. A significant part of the electrochemical biosensors are based on the semiconductor technology. Silicon-based biosensors- as a field of electrical biosensors have gained much attention for several decades, mostly in bioanalytical applications, since they are favorable for their high sensitivity, miniaturization, speed and low cost. Several research group conducted studies that have examined biological events, like protein-protein interactions, antigen-antibody binding, enzyme-substrate reactions and nucleic acid hybridizations based on the usage of silicon-based biosensors [38].

Most reported EnFETs (enzyme-modified field-effect transistors) are built-up of pH-sensitive ISFETS. Examples are EnFETs for the detection of glucose, urea, penicillin, organophosphorus pesticides, creatinine, phenolic compounds, glycoalkaloids, etc. [39]. Another aspect of electrochemical biosensors is the „cell/FED” hybrids. Their major applications are monitoring of electrical communication within neuron networks, transmission path of ionic channels. Also it is used as biosensor to monitor toxic substances, pollutants, pharmaceutical agents, etc.

Not only research groups are interested in the development of different biosensors, biosensing devices. Figure 8 gives a brief lists about companies and their inventions.

Company	Product	Cell-Based Assays
a, Applied Biophysics	ECIS	Cell adhesion, proliferation, barrier function, receptor-mediated signaling, and wound healing
b, ACEA Biosciences and Roche	xCELLigence (RT-CES)	Cell adhesion, proliferation, cytotoxicity, receptor-mediated signaling, barrier function, cell migration, and invasion
c, Bionas	Bionas 2500	Cell adhesion, proliferation, metabolism, and cytotoxicity
d, MDS Sciex	Cellkey	Cell adhesion, proliferation, receptor-mediated signaling

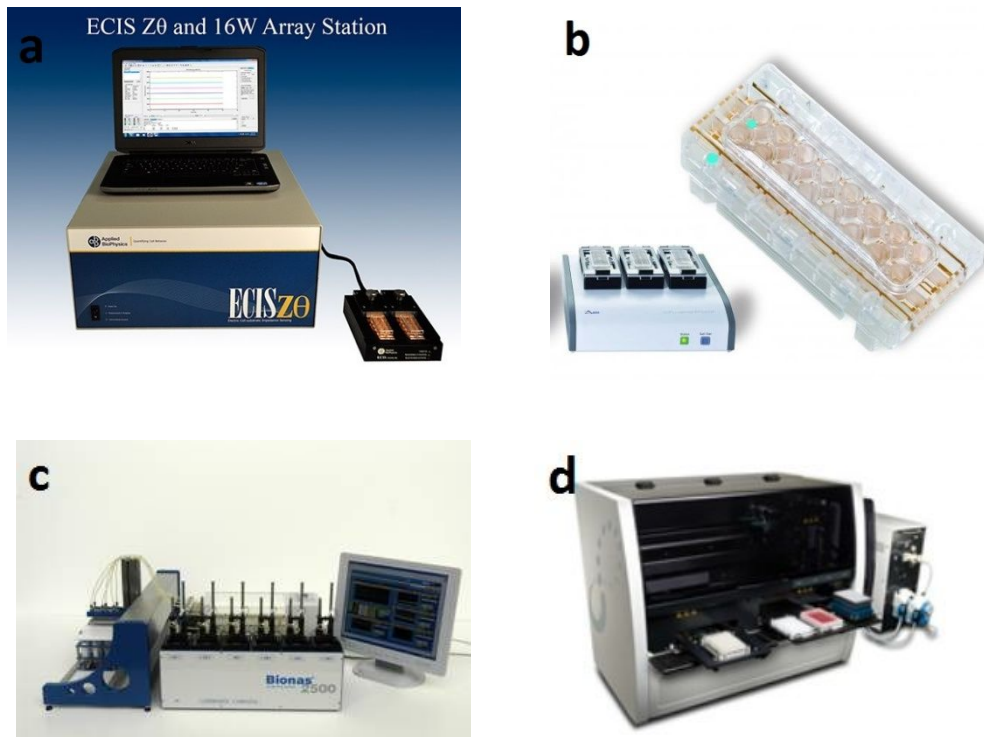


Figure 8.: Different commercially available biosensing devices. A, Electric Cell-substrate Impedance Sensing (ECIS) for real-time, label-free, impedance-based method to study the activities of cells grown in tissue culture. B, xCELLigence is used to monitor cell proliferation and viability. C, Bionas 2500 monitors physiological parameters of living cells and tissue slices. D, Cellkey is a functional cell-based assay technology with high sensitivity to measure endogenous receptor targets in whole live cells.

4. Organ-on-a-chip devices

Organ-on-a-chip is a microdevice developed to represent the physiological functions of tissues and organs by using living cells [40]. These chips contain cells that can be cultured with continuous perfusion inside a micro-sized chamber on the chip. They are able to integrate physical forces, including physiologically relevant levels of fluid shear stress, cyclic strain and mechanical compression, and permitting analysis of organ-specific responses. Furthermore, the development of organ-on-a-chip with *in vitro* cell barrier models can be used to study parameters that control permeability and predict drug transport across these barriers in the early stages of drug discovery. The growing interest in organ-on-a-chip system is due to their potential for providing a high throughput, cost-effective and reliable method for predicting drug interactions in humans including transport phenomena.

The microfluidic chips provide control over many system parameters such as fluid flow in the channels. This allows the generation of physical and chemical gradients, which has been utilized for noninvasive study of directional cell migration, cardiac tissue formation as well as nerve axon outgrowth. Fluid shear stresses can be controlled independently of physical and chemical gradients by altering flow rates or channel dimensions. Control of cell patterning is another useful feature. By using laminar streams, designing complex microchannel paths or positioning microposts between neighboring cell types ensure the appropriate cell arrangement. In recent years, organ-on-a chip has gained increasing attention due to both ethical and scientific reasons. It has a great potential for providing high fidelity, cost-effective and reliable method. But still the most important advantage is that with this device the number of animal experiments can be reduced [41]. Several promising organ-on-a-chip systems have been developed by different research groups, such as blood-brain barrier[42], gastrointestinal tract model [43], human gut-on-a-chip [44], lung on a chip [45], liver on a chip [46].

4.1. Placenta-on-a-chip - an expanding microdevice

There has been conducted a wide range of studies to establish different in vitro, ex vivo and animal models in order to gain a better insight into the function of the placenta. While coping with the limitations of these models researchers changed their direction of interest of placenta experiments towards “organ-on-a-chip” technology. The goal of designing a placenta-on-a-chip is to provide increasing accuracy in drug testing model to study drug delivery to the placenta. In this section, two recently developed placenta-on-a-chip will be described.

Lee et al. developed a placenta-on-a-chip using soft-lithography technique. The microchannels were created by PDMS separated by an extracellular matrix (ECM) membrane. JEG-3 placenta cells were cultivated on the apical site of membrane, endothelial cells on the lower site and under dynamic condition the glucose transport was measured in order to analyze the physiological function of the microengineered placental barrier. This device provides simulations and examinations various physiological responses of the placenta barrier [25].

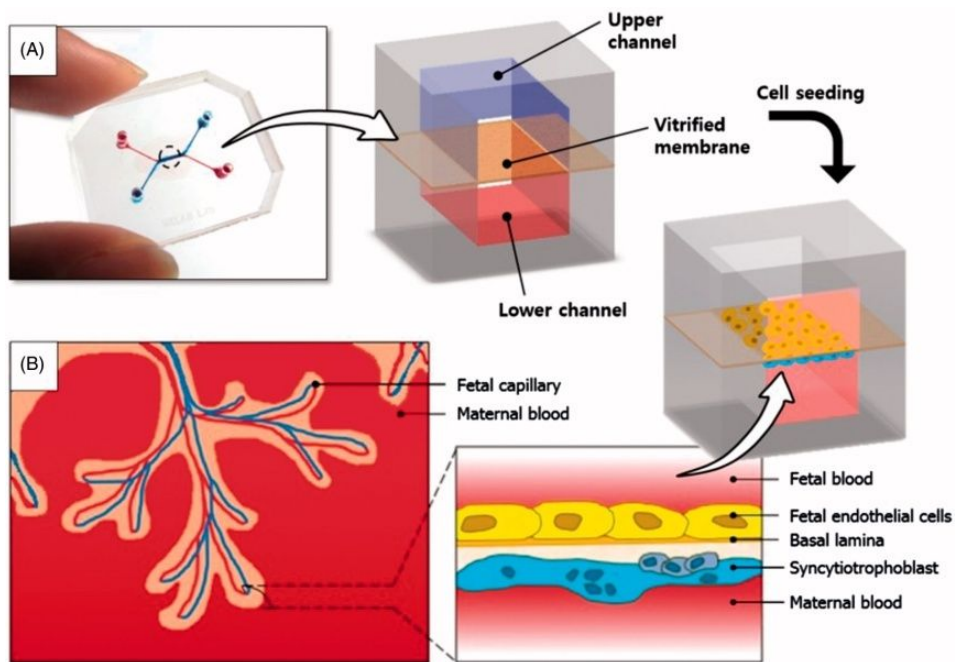


Figure 9.: Placenta-on-a-chip. A. The upper and lower channel of the device is separated by a vitrified collagen membrane. B. Endothelial cells and trophoblasts are co-cultured on each site of the membrane mimicking a placenta barrier.

The second microdevice was established by Huh et al. They invented a similar chip design as the research group of Lee and by culturing of B30 and endothelial cells onto each side of the membrane glucose transport were monitored.

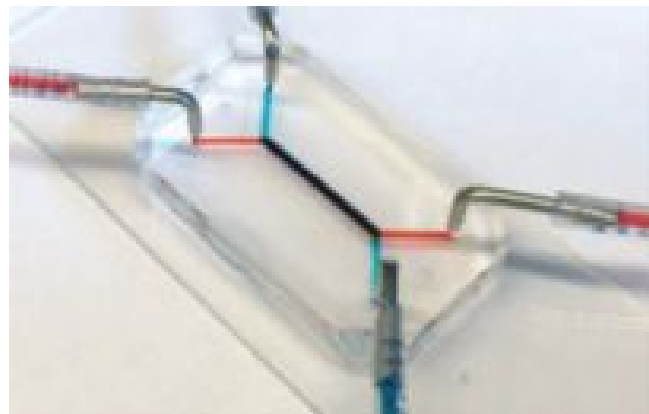


Figure 10.: The microdevice was fabricated by soft-lithography technique. Microchannels were created by PDMS with a channel dimensions of 1mm (width) x 1.5 cm (length) x 135 μ m (height).

Furthermore this device is capable of simulating the extracellular microenvironment, while digitally visualizing, quantitatively analyzing human-specific placental structure and function [47].

4.2. Transepithelial/endothelial electrical resistance measurements (TEER)

Trans-epithelial endothelial electrical resistance (TEER) is a useful method to study the performance of the cell growth in organ-on-a-chip devices. Endothelial and epithelial cells are connected to each other via intercellular junctions such as adherent, gap and tight junctions. Tight junctions perform vital functions such as keeping the cells together, regulating diffusion between cells, helping to maintain the polarity of cells and sealing the endothelial cell layer. With the measurement technique of TEER the integrity of tight junction dynamics in cell culture models of endothelial and epithelial monolayer can be measured. Barrier integrity is vital for the physiological activities of the tissue. TEER measurement has been carried out on different cell types both with custom build microfluidic implementations and commercially available devices. The main advantage and wide use of this method is because it can be applied non-invasively to monitor living cells during their different growth stage and differentiation [48]. The commercially available devices for measuring TEER are conditioned to static and macroscopic cellular environments, as the diameter of the culture wells are 12 mm. The in vitro models should also incorporate apical as well as basolateral compartments with appropriate composition of the aqueous medium on each side of the cell membrane. Lippmann et al. have developed a better mimetic model by demonstrating the derivation of brain endothelial cells from human induced pluripotent stem cells. They applied various methods to evaluate the structural and functional properties of the blood-brain-barrier model [49]. Furthermore a complex 3D in vitro model of physiologically relevant human upper airways was developed using Calu-3 epithelial cells, MRC-5 fibroblasts and dendritic cells grown on scaffolds. This model allows monitoring of the cellular signaling of airway epithelia to elucidate potential mechanism of small airway disorders [50].

Schoen et al. cultivated oviduct epithelial cells on porous membrane. TEER measurements were conducted to monitor the quality of the cultivation. Moreover the correlation between the cellular height and TEER in fully differentiated routine cultures was analyzed. This research showed that there is a negative correlation between TEER and cellular height. This parameter reflects the degree of apical-basal polarity and TEER that's corresponds to the strength of cellular junctions [51].

5. Theoretical Background

5.1. Impedance of cells

Due to the electrical properties of mammalian cells, they can be investigated by electrophysiological approaches. The electric properties of a cell are influenced by the plasma membrane and the cytosolic electrolytes. A mammalian cell is surrounded by semipermeable plasma membrane acting as a protector and separator shell from its environment. It consists of two lipid monolayers by the opposition of their hydrocarbon chains [52]. The polar 'head' groups are oriented to the intra- and extracellular aqueous liquid and isolate the hydrophobic lipid 'tail' from water. This is a requirement for the cells resting potential and ensures their passive electrical properties. The cell membrane exhibits an imbalance of electric charges between its positively charged inner, and negatively charged outer side to yield the membrane voltage u .

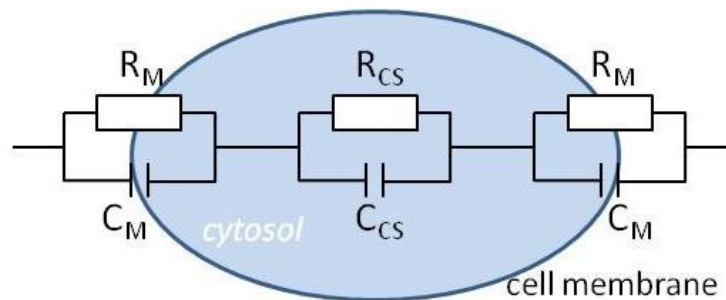


Figure 11.: Electrical model of the cell. The cytosol can be modeled by a capacity and a parallel resistance, due to the intracellular membranes such as nucleus and mitochondrium furthermore other protein complexes.

The dielectric nature of the membrane combined with the thickness of the membrane itself ensures the highly capacitive behavior. This can be modeled with a simplified electrical behavior, taking into consideration that the value is dependent on the cell type and the surrounding media. The capacity C_M (~ 0.8 pF) dominates at the membrane due to the high membrane resistance R_M ($\sim 4G\Omega$) [53]. The intrinsic electrical conductance of the

phospholipids bilayer is very low and therefore it can be considered as an insulator [54]. It works as filter, passing AC but blocking direct current. Charge will accumulate on one side of the capacitor while applying a DC voltage across it. The electric field indicated by the accumulated charge is the source of the impedance to the flow of current. Driven by an AC supply, a capacitor will only accumulate a limited amount of charge before the potential difference changes sign and the charge dissipates. The applied frequency is inversely proportional to the amount of accumulated charge and to the impedance to the flow of current. Furthermore, in case of the applied current having a sufficiently high frequency, the current can capacitively couple through the plasma membrane along the transcellular pathways. However, at most frequencies, the AC signal passes between the cells and the electrode surface through the narrow channels since it cannot penetrate the cells due to the low capacitance [54]. Thus, the current cannot flow from the electrode to the bulk electrolyte, and the effective area available for the current is limited. If the cell density on the electrode surface is high, it causes an increase in the impedance values.

The electrical impedance therefore conveys information about the cell population. The body can be considered as a composite volume conductor consisting of a bunch of tissues with different electrical properties. Conductivity and relative permittivity varies not only in different cell types but also with the frequency of the applied field. The permittivity is related to the extent to which the bound charges can be displaced or polarized under the influence of the electric field. A dielectric dispersion can be observed in tissues in which the relative permittivity decreases with increasing frequency. Three types of dispersions can be distinguished. Alpha dispersion: 10 Hz to a few kHz, associated with tissue interfaces, membranes. Beta dispersion: 1kHz to several MHz, associated with the polarization of cellular membranes, proteins and further organic macromolecules. Gamma dispersion: > 10GHz is associated with polarization of water molecules. Since the cellular impedance is determined by the dielectric properties of the plasma, the frequency range of beta dispersion is the most interesting for the investigations [55].

5.2. Transepithelial/endothelial electrical resistance measurement according to Ohm's law

Transepithelial/transendothelial electrical resistance (TEER) is a widely used quantitative technique to measure the integrity of tight junction dynamics in cell culture models of endothelial and epithelial monolayers. Tight junctions connect adjacent cells, control the passage of molecules across the barrier and furthermore facilitate active transport processes [48].

The so-called Voltohmmeter is a simple device, with two chopstick-like electrodes, widely used to measure TEER. In this method two compartments are distinguished by a porous semipermeable membrane, on which cellular monolayer is cultured. The use of conductive liquid is essential to carry out measurement. One electrode is placed in the upper compartment (apical) and the other in the lower (basolateral). AC voltage signal with square waveform at frequency 12.5 Hz is applied and the current is measured. This frequency is required in order to not to leave a charge behind on either the electrodes or the membrane. The periodic measurement of the well is a plot of the growth of the cells on the membrane by a resistance measurement. The membrane has reached confluence, as soon as this resistance graph has plateaued.

With this method the cell specific resistance (R_{tissue}) can be determined by the resistance value across the cell layer on the membrane (R_{total}) and by the blank resistance (R_{blank}) of the membrane without cells:

$$R_{\text{tissue}}(\Omega) = R_{\text{total}} - R_{\text{blank}} \quad \text{eq(1).}$$

TEER values are calculated in units of Ωcm^2 with the help of the effective area of the semipermeable membrane:

$$\text{TEER} = R_{\text{tissue}}(\Omega) * M_{\text{area}}(\text{cm}^2) \quad \text{eq(2).}$$

The confluence of the cellular monolayer can be detected by an increase in TEER. However due to the easy and fast operation of the Voltohmmeter, its application for permeability studies should be considered. Due to the following drawbacks there is a significant risk of

obtaining wrong results: first of all, the resulting TEER value depends on the position of the electrodes. It can be explained by the motion of the electrodes that can cause disturbances and disruption of the cell layer.

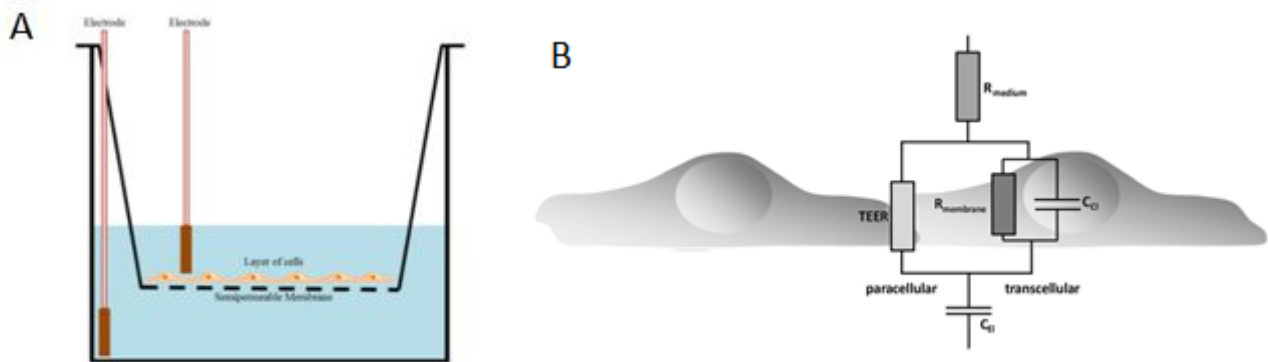


Figure 12.: Schematics of TEER transwell Volttohmmeter. B, equivalent model of the cellular barrier.

Furthermore systematic miscalculation of TEER can occur by the inherent inhomogeneity of the electric field across the cell layer. In many cases, the chopstick electrodes are not suitable for integration with body-on-a-chip systems due to the small cell culture area. An equivalent circuit and corresponding mathematical models are able to characterize the cellular barrier properties accurately. The current flows through the paracellular route (junctions between the cells) and through transcellular route (membrane of the cells). The tight junctional proteins represent an ohmic resistance (TEER) and the lipid bilayer can be described as a parallel circuit of an ohmic resistance ($R_{membrane}$) and an electric capacitance (C_{cl}). This circuit can be simplified by the fact that the lipid bilayers can be represented with just C_{cl} . The current flows mostly across the capacitor due to the high values of $R_{membrane}$, so the membrane impedance can be neglected [56]. Typically, the impedance spectrum can be divided into three significant regions, according to the equivalent circuit element that is dominating the impedance. In the low frequency range, the signal is dominated by C_{el} , in the mid frequency range by R_{TEER} and C_{cl} , that are the elements related to the cells. Furthermore in the high frequency range C_{cl} and C_{el} provide a more conductive path and the impedance is dominated by R_{medium} .

5.2.1. Electrode configuration for transepithelial/endothelial electrical resistance measurement

The electrode consists of a fixed pair of probes, each with an outer and inner electrode. The outer electrodes with small silver pads pass current through the membrane sample. The inner electrodes, voltage electrodes, are Ag/AgCl pellet voltage sensors. It is designed to make measurements of the membrane voltage and resistance of cultured epithelial in tissue culture wells. [57].

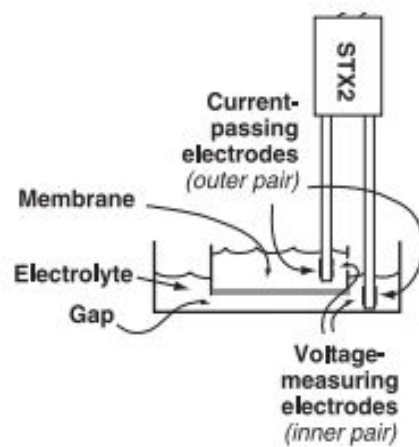


Figure 13.: Working principle of the EVOM2 VoltOhmmeter. Placement of the electrode is a critical point in order to make accurate measurements. Reproducibility of the measurements can be improved by positioning the longer tip so that it touches the bottom of the dish each time.

5.3. Impedance spectroscopy

More reliable measurement method to measure transepithelial/endothelial electrical resistance is impedance spectroscopy. AC signal with a small amplitude and frequency sweep is applied while measuring the amplitude and phase response of the resulting current. The resulting complex impedance Z provides information about the capacitance of the cell.

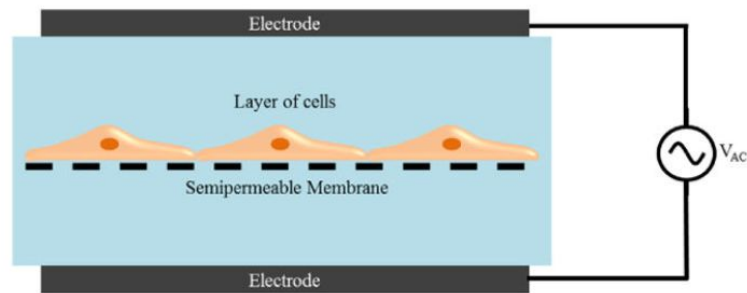


Figure 14.: Schematics draw of electrical impedance spectroscopy

5.3.1. Two- and four electrode impedance measurement setup

Different electrodes and measurement setups are used in impedance measurement. Working electrode is made of an inert material such as Pt, Au, graphite, glassy carbon. The current is flowing between the working and counter electrode, thus the surface area of the counter electrode has to be higher than the area of the working electrode. Reference electrode is used as a point of reference in the system for potential control and measurement [58]. The counter electrode is also made of similar inert material such as Au, Pt, glassy carbon etc.

The most basic form of a cell comprises two electrodes immersed in an electrolyte. CE and RE are shorted on one of the electrodes, which allow the current to pass through the cell. WE and S are shorted on the other one, so the interface between electrolyte and electrode is investigated. The potential across the complete cell is measured. Applying a potential across the electrodes causes a current to flow through the cell. This kind of measurement method is preferred when the behavior of the whole cell is under investigation. The setup is typically used with energy storage or conversion device like bacteria or fuel cells etc. It is also used in measurements of ultrafast dynamics of electrode processes or electrochemical impedance measurements at high frequencies (> 100 kHz).

Four electrode cell setup is used where the potential difference between reference and S need to be measured. This difference is caused by a current across a well defined interface – between working and counter electrode. For example while measuring the junction potentials between two non miscible phases or across a membrane. This enables to calculate the resistance of the interface or the membrane conductivity [58].

6. Materials and Methods

6.1. Cell culture basics

6.1.1. Cultivation of placenta cells

Human placenta carcinoma cells (JEG-3, JAR, ACH-3P, ATCC, BeWo-B30) were obtained from Medical University of Graz and cultivated in T75 cell culture flasks in a suitable cell incubator at 37°C in a 5% CO₂ environment. Different media were used for the placenta lines, according to the nutrition the cells require.

Name of the cell line	Cultured medium	Medium short name	Supplementary
ACH-3P, BeWo ATCC, BeWo-b30	DMEM/Ham's F12 1:1 (1X) Containing 2mM L- Glutamine	DMEM+	2mM L-Glutamine 1% Pen-Strep 10% FCS
JAR-G	RPMI 1640 (1X) Containing 2mM L- Glutamine	RPMI+	1% Pen-Strep 10% FCS
JEG-3	MEM (Eagle) Containing 2mM L- Glutamine	MEM+	1% Pen-Strep 1 mM Sodium Pyruvate 1% non-essential amino acids 10% FCS

Cells were split twice a week (1:3) in order to avoid high cell confluence in the flask. The medium was removed carefully from the flask by a pipette. In order to get rid of the non-living cells, the T75 flask was washed out with 5 ml sterile PBS twice. Then, 2 ml trypsin was introduced into the flask and was placed in the incubator for 10 minutes for enzymatic cell removal. The trypsin, already containing the cells, was transferred into 15 ml sterile flask

with a pipette, and 5 ml medium was added to in order to inactivate the trypsin. After the cells were centrifuged for 5 min at 140 relative centrifugal force (rcf), a pellet could be observed at the bottom of the tube. Trypsin was carefully removed from the tube and the pellet was homogenized by 1 ml medium after which 2 ml medium was added. Three new T75 flasks were filled with 12 ml medium, and the 1 ml cell suspension was divided equally into each flask and placed into the incubator.

6.1.2. Cell counting method

Cell counting was performed before each experiment using Neubauer chamber. The cell number was calculated by the following equation, after the cells were counted in the outer four squares of the device.

$$N = \frac{n}{q} * d * V * f,$$

where n is the number of the counted cells, q the number of the counted squares, d the dilution factor, V the total cell suspension volume and f the volume factor, for this chamber is 10^4 .

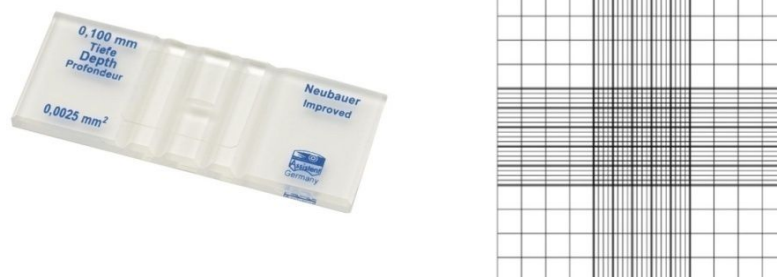


Figure 15.: Neubauer chamber for cell counting, performed under the microscope.

6.1.3. Cell characterization

Five placenta carcinoma trophoblast cells were examined in this work, provided from the Medical University of Graz. JAR, BeWo and JEG-3 cell lines are derived from trophoblastic tumors of the human placenta. JEG-3, derived originally from the BeWo, express abundant human chorionic gonadotropin and placental lactogen- hallmarks of trophoblasts- and form

large, multinucleated syncytia in culture which resemble that of syncytiotrophoblasts *in vivo* [59]. BeWo b30 cells are derived from a human choriocarcinoma that has retained cell properties and hormonal profiles of mononucleated cytotrophoblasts. The b30 BeWo clone has a monolayer forming ability and has been used to study placental distribution of drugs and nutrients [60]. ACH-3P is a first trimester trophoblast cell line, immortalization of the cell was established by fusion of primary human first trimester trophoblast (12 week of gestation) with a human carcinoma cell line (AC1-1). ACH-3P showed a uniform polygonal, epithelial-like cytomorphology [61]. The JAR cell line shares many early placental trophoblast cell characteristics, such as synthesis of human gonadotropin and steroids, and the ability to differentiate into syncytiotrophoblast-like cells *in vitro* [59].

6.2. Viability test

Viability experiment was carried out with 48 well plates with a working volume of 200 μ l, and a growth area of 1.12 cm² was used. In order to obtain faster and more effective cell adhesion, the surface of the well plates was treated with 1% gelatine (diluted in sterile 1x PBS) and incubated for 1 hour. The gelatine was washed out properly the medium from the wells with before cell seeding.

JEG-3, JAR, ACH-3P, ATCC, BeWo-b30 cell lines were used. The cells were dissolved from the wall of the T75 flask as described above and after homogenization, the amount of each cell type was determined with the Neubauer chamber. Cell suspension was diluted to 1.25×10^5 /ml. Three wells were filled up with the same cell type, each well contained 2.5×10^4 cells (200 μ l). The plates were placed in the incubator for 24 hours to adhere. Images were taken of the cells with microscope (20x). Colchicine, chlorpromazine and methylmetanosulfanate (MMS) solutions were prepared and diluted in the medium to (EC50 value) 500 μ M. The medium was replaced by poisons in each well and placed into the incubator. After 4 hours exposure time images were taken of each well by a microscope (20x). Presto Blue cell viability reagent was used to analyze cytotoxicity on the cells. The poisons were replaced by 500 μ l presto blue dye (10% v/v in complete medium). For this process, the light of the laminar was switched off. The plates were covered with aluminum to avoid exposure to direct light and were placed in the incubator for 30 minutes. Images were taken of each well. The 200 μ l Presto Blue supernatant was removed from each well

and 100 µl placed in a new 96 well plate as duplicates. In order to define the cell viability, fluorescent measurements were carried out by plate reader device. CellGen software was used with the following setup: with lid, fluorescence: 560-590nm, bottom read, gain 100. Data was exported to Excel for further analysis.

During the second attempt BeWo-b30 and ATCC cells were used with the concentration of $1.25 \cdot 10^6$ cells/ml. Colchicine and methyl solutions were prepared and diluted in DMEM+ to 1000µM and chlorpromazine was diluted in sterile distilled water to the same concentration. Each solution was further diluted and the medium in the wells was changed to the appropriate poison concentration according to the table below. After that, the same process was carried out, as already discussed above.

1000	1000	1000	0
500	500	500	0
250	250	250	0
125	125	125	15,625
62,5	62,5	62,5	15,625
31,25	31,25	31,25	15,625

Further viability test was carried out on ATCC and BeWo-b30 cells with SiO₂ nanoparticles. In this case, 48 wells were filled with 40000 cells. After 24 hours seeding the medium was replaced by NPs. After 4 hours of incubation, the cells were dyed with 10% Presto Blue. For this experiment, each well was filled with 150µl Presto Blue. After 30 min, 100µl Presto Blue was removed from the wells and transferred to a new well plate.

500	500	500	0
250	250	250	0
125	62,5	125	0
62,5	62,5	62,5	0
31,25	31,25	31,25	0
16,625	16,625	16,625	0

6.3. Transepithelial/endothelial electrical resistance measurements

6.3.1. Characterization of the measurement method

TEER measurements were carried out with EVOM2 VoltohmMeter, purchased from WorldPrecision Instrument with 12 well plate transwells, working volume of 500 μ l, total volume of 2 ml.

TEER measurements were carried out according to Fei et al.[23]. JEG-3, JAR, ACH-3P, BeWo-b30, BeWo-ATCC cell types were used at the concentration of 2×10^5 cells/ml. Transwell well plates with 12 well/plate were used for the experiment with the working volume of 500 μ l, total volume of 2 ml. The inner wells were filled up with 10^5 cells (500 μ l) and the outer wells with 1.5 ml medium, according to the cell types. On the day of seeding impedance measurement was carried out with EVOM2. Further TEER measurements were conducted on the 1st, 3rd, 5th and 7th day according to the following protocol. The plate was taken out of the incubator and stored in the sterile work bench for 40 minutes to cool down the wells to room temperature. This step is required in order to avoid the fluctuation of the temperature. The medium of one well was exchanged to a new one for each cell type, and TEER was measured in the new medium. The other wells were also filled up with new medium after washing them out 3 times with sterile PBS. TEER was measured in the new medium. After the measurement, the plates were stored in the incubator at 37°C.

TEER measurement was carried out, JEG-3, Jar, ACH-3P, ATCC, B30 cell lines were used. 100.000 cells were seeded into each well. The medium was not changed during the experiment. The well plates were stored in the incubator, before measuring TEER, plates were taken out of the incubator, and placed in the laminar for 40 min. TEER was measured on day 0, 1, 3 and 5. On the 5th day, the medium in the wells and also in the outer chamber was replaced by different poisons that have been already used for viability tests. The used concentrations for colchicine, methyl 500 μ M, chlorpromazine: 120 μ M. The experiment was carried out also with 50.000 cells/well and 25.000 cells/well. TEER was measured after 4 and 24 hours of poisons exposure.

TEER measurement was repeated also with SiO₂ nanoparticles. On the 5th day, medium was replaced by different concentrations of NPs (according to the table below) and TEER was measured after 4 and 24 hours of exposure.

500	500	500	0
250	250	250	0
125	125	125	15,625
62,5	62,5	62,5	15,625
31,25	31,25	31,25	15,625

6.4. Chip design considerations for impedance spectroscopy

6.4.1. Blank chip for monitoring cell morphology

A blank chip was developed in order to monitor the long-term cell morphology. Adhesive tape was used to build a 3D complex biochip. The design of the microfluidic channel was drawn with AutoCAD. Using rapid prototype technology the channels were cut by a 3D plotter. Two microscope glass slides were used as substrate.

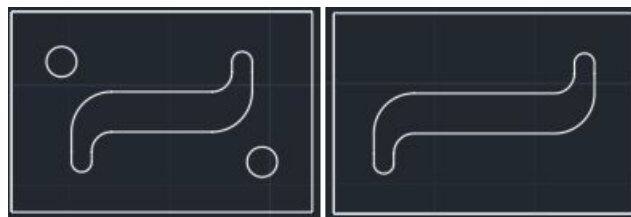


Figure 16.: Channel design of the first microfluidic chip to carry out cell adhesion measurements.

According to the design, four holes with the diameter of 1 mm were drilled into the upper glass serving as microfluidic in- and outlets. The substrates were cleaned and dried properly. They were submerged into Hellmanex solution and placed into ultrasound bath for 10 minutes at room temperature. Thereafter the glasses were put into Isopropanol absolute and rinsed with distilled water. They were dried carefully with nitrogen gun and placed into the oven for 10 minutes at 70°C. The adhesive tape layers were glued onto the surface of the

glasses. 1 cm long polymer tubes (IDEX Health & Science Tygon) with the inner diameter of 0.76 mm were glued by two component glue to the glass and placed in the oven for 20 minutes at 70 °C to harden.

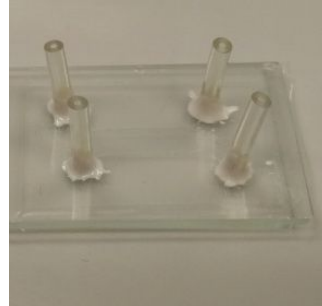


Figure 17.: Assembled blank chip with adhesive tape and polymer tubes to ensure microfluidic flow for cell adhesion measurement.

6.4.2. Characterization of PDMS bonding

The experiment was carried out with glass and PDMS with different power and duration of the plasma exposure. The surface of the glass was cleaned properly, as discussed above. 250 μm thick PDMS sheet was washed with soap, rinsed with isopropanol and distilled water. It was dried with a nitrogen gun. After performing a plasma treatment, the activated surfaces of glass and PDMS were pressed strongly together by hand and also by pliers, and placed into convection oven for 10 minutes at 70°C. Bonding test was performed on every substrate by tweezers.

6.4.3. Coplanar chip for impedance measurement

A new electrode design was developed with coplanar electrodes. Chips with seven electrodes were manufactured at the Solid State Electronics department at the TU Wien using photolithography. 20 nm Cr and 200 nm Au layer were deposited with lift-off process. Electrodes and microscope slides were cleaned properly. 250 μm thick PDMS layer was used, the channel arrangement was drawn by AutoCAD and the design was cut by a cutter. A microscope slide was used as a cover glass. Holes were drilled into the glass at the appropriate spot in order to ensure the microfluidic flow.

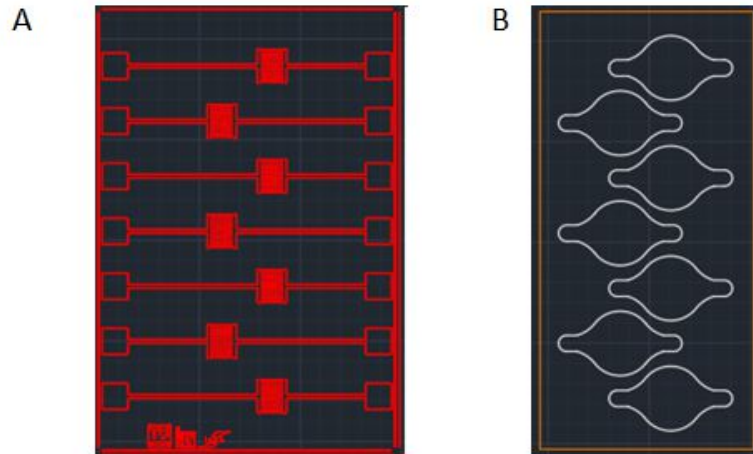


Figure 23.: AutoCad design of the electrodes and microfluidic channel. A, each chip consisted of seven sensors in order to carry out parallel measurements. B, additional AutoCad design was made for each sensor to ensure a well defined microfluidic channel for the cells.

The glass was bonded to the PDMS according to the protocol. Microfluidic in- and outlet ports were fixed to the glass, as described above.

6.4.4. Final coplanar electrode design

The same electrode design was used to the new chip configuration. PDMS was poured by mixing PDMS and poured to the ratio of 1:10 in a big petri-dish. It was left overnight to harden. The chip was build together according the process mentioned above.

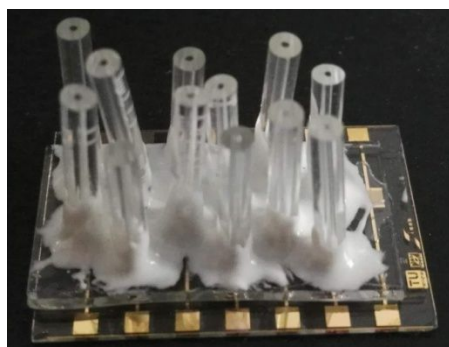


Figure 18.: Final chip design for electrical impedance measurement. This PDMS thickness (3 mm) was not suitable for the cutter; therefore the channels were cut out by hand, using a standard, in order to get equal size.

6.5. Placenta station for cell adhesion measurement

The placenta station was assembled in order to carry out long-time electrical impedance spectroscopy measurements on the chip. A portable, heat-able plate was built as a platform.

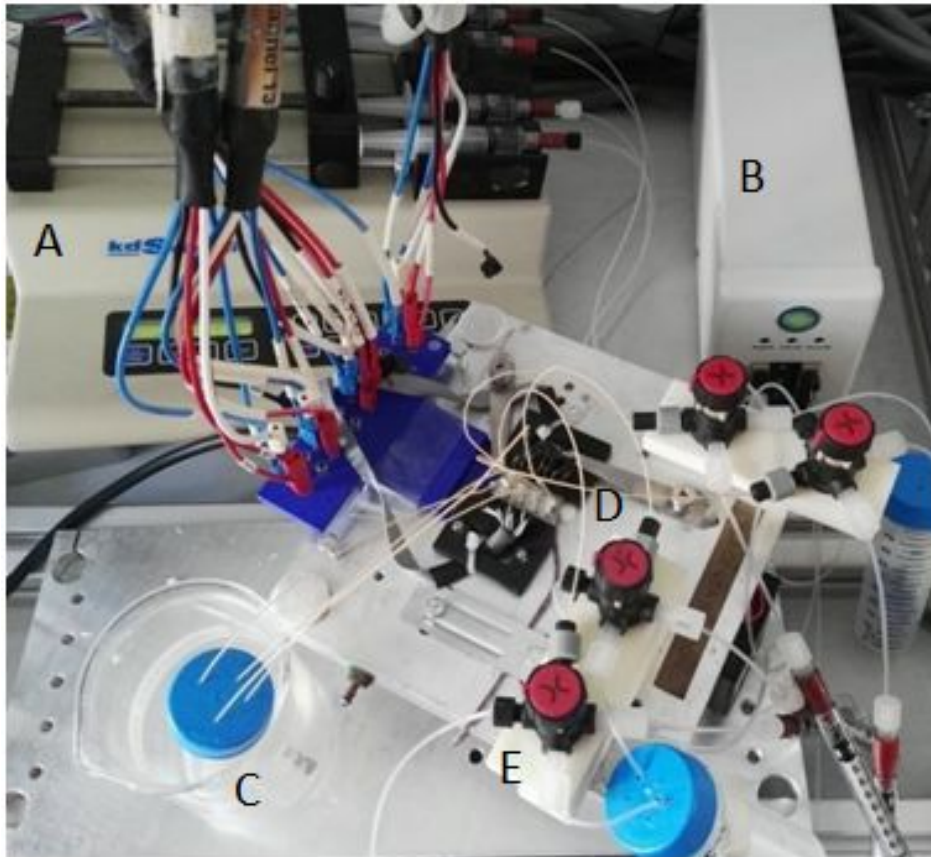


Figure 19.: Placenta station with syringe pump (A), degaser (B), waste (C), chip fixed by springs and screws (D) and valves (E) to ensure a bubble-free injection of the cells .

The chips are fixed onto the platform by screws. The connection between the measurement channels of potentiostat and the electrode ports were made by adjustable conductive springs. These springs were fixed to the supporting element, designed by AutoCad. A syringe pump was connected to the inlet of degaser device; the outlet of the degaser was connected to the valve system. The 2-state valve could be switched to the inlet of the microfluidic channel and to the waste.

6.6. Placenta barrier integrity measurement

6.6.1. Measurement characterization

The chip was fixed to the pre-heated placenta station. The inlet ports were connected together with the valves, and the outlet ports with the waste, to ensure continuous flow through the channel. Ethanol was rinsed through the channels for 1 hour to sterilize. In order to achieve better cell adhesion, gelatine coating was applied on the surface of the chip. After 30 minutes, the gelatin was replaced by MEM+ medium. JEG-3 cells were used for this measurement and prepared as discussed above. After a stable baseline was reached by the medium, the pump was stopped and JEG-3 cells (10^6 cells/ml) were injected into the system through the valves. The flow was started again after different adhesion times: 4, 14 hours. Trypsin was injected, to wash the cells away from the surface of the chip.

6.6.2. Cytotoxicity test of ATCC and B30 cell-lines

The preparation, sterilization and improvement of the surface adhesion by gelatine were achieved in similar way as discussed above. For these measurements ATCC and B30 cells were used. The flow rate was set to 4 μ l/min. The system enables to measure four channels simultaneously. When a stable base line of the medium was achieved, the flow was stopped. 10^6 cells/ml was injected into each channel. After 14 hours of cell adhesion, the pump was turned on, and medium was driven through the channels with the velocity of 4 μ l/min. 24 hours after cell injection, the medium of three channels was replaced by the poisons that have been already used for the viability test and the TEER measurements. The fourth channel was measured only with medium. Different concentrations were used for each cell type: MMS 500 μ M, chlorpromazine 120 μ M.

7. Results

7.1. Characterization of cell morphology

Cells were cultivated in medium with 10% FCS. The endothelial cells of all five cell lines rapidly attached and spread upon the transwells. Cells require medium with different protein, glucose and hormone content. Therefore population doubling times varied in a wide spectrum, according to the nutrition they needed [62].

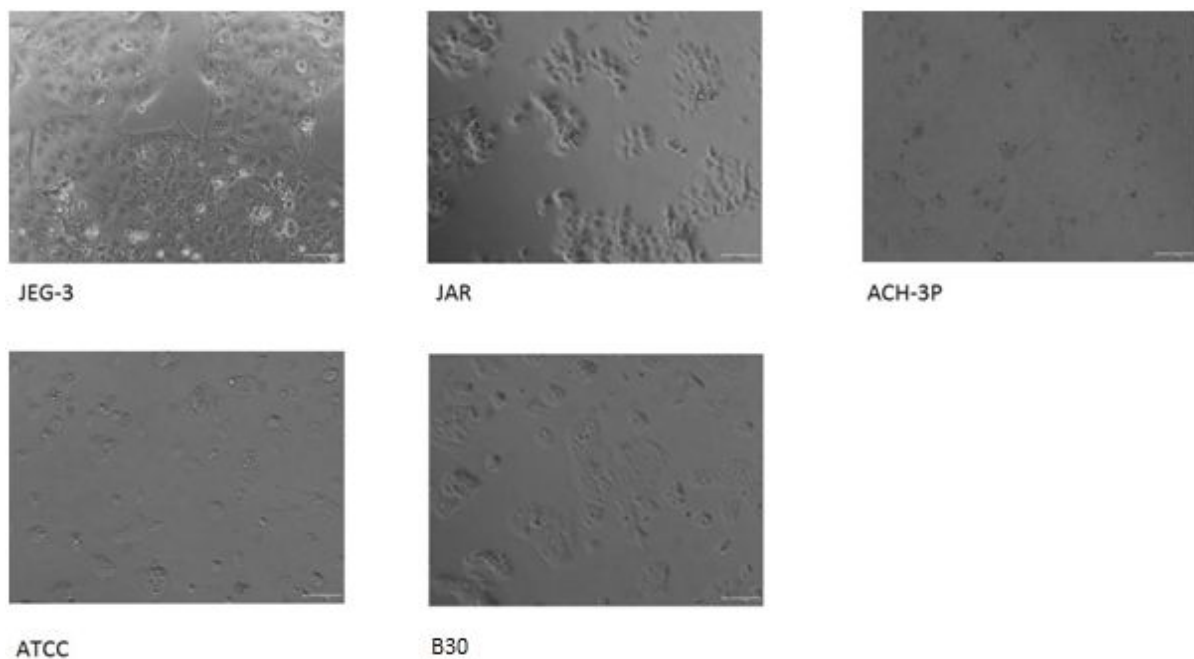


Figure 20.: Different cell lines cultivated in 48 transwells. Seeding density was $2.5 \cdot 10^4$ cells/well. After 24 h seeding, the cells are attached on the surface and started to proliferate.

They formed large, connecting clusters, and tight epithelium. However, they are derived from placenta, morphology, size and growth factor differs among the cell lines. Figure 20 shows that JEG-3, ACH, ATCC cell lines grow rapidly, forming a complex 3D multilayer. On the other hand JAR and B30 cells form monolayer. Due to differences of growth rate, the rate of the confluency varies between the cell lines.

7.2. Cytotoxicity test on placenta cell lines

7.2.1. Cytotoxicity test of colchicines, chlorpromazine and MMS

End point cytotoxicity assay was carried out in order to monitor the effect commercially available medicines, namely methylmetanosulfate (MMS), colchicine and chlorpromazine. Time and cell-dependence of toxicity was monitored in order to analyze the quality of tight junctions formed by different cell lines. Five different placenta cells were used in order to examine the effect on the cells with different morphology (two- and three dimensions cell layer). The experiments were performed in triplicates. The normalized values are shown on Figure 21, 22 and 23. After 4 hours of colchicine exposure the highest cell viability was yielded to B30 with $92\pm 2.6\%$ and to ACH with $88\pm 7.4\%$ (Figure 21). The rate of the living cells was $77\pm 6.3\%$ for ATCC, $67\pm 4.2\%$ for JEG-3 and $51\pm 5.9\%$ for JAR, respectively. After 24 hours the viability of B 30 was further reduced by 39% ($53\pm 4.5\%$), ACH by 49% ($39\pm 4.8\%$) and ATCC by 13% ($38\pm 7.3\%$). Furthermore the ratio of non-viable JEG-3 cells was $24\pm 3.3\%$ and for JAR $43\pm 5.9\%$. MMS exposure decreased cell viability to $77\pm 6.5\%$ for B30 cells, to $58\pm 6.5\%$ for ACH, to $62\pm 4.3\%$ for JAR and $65\pm 4.5\%$ for JEG-3 after 4 hours (Figure 22). The values were further decreased after 24 hours of exposure time. $43\pm 5.8\%$ cell viability was observed for B30 and $45\pm 2.1\%$ for JAR. Similar cell viability was shown by ATCC, JEG-3 and ACH, namely $38\pm 6\%$, $32\pm 8.4\%$ and $31\pm 9.7\%$. The lowest ratio of the viable cells was yielded to the effect of chlorpromazine (Figure 23). After 4 hours of exposure only the fifth of the cells were metabolically active for all cell lines. B30, JAR and ACH showed nearly same viability rate: JAR $19.8\pm 1.2\%$, B30 $18.4\pm 2.3\%$, ACH $17.5\pm 3.1\%$. $15.4\pm 2.4\%$ of JEG-3 was alive and $14.9\pm 2.5\%$ of ATCC, respectively. After 24 hours, the rate of the apoptotic cells extended above 90%. The highest mortality rate was observed at JAR and ACH cell lines (96.8 and 96.4%) followed by ATCC with the rate of $95.6\pm 0.5\%$ and by JEG-3 with $92\pm 1.4\%$. B30 cells were the most resistance, $98\pm 0.2\%$ % of the cells was metabolic active.

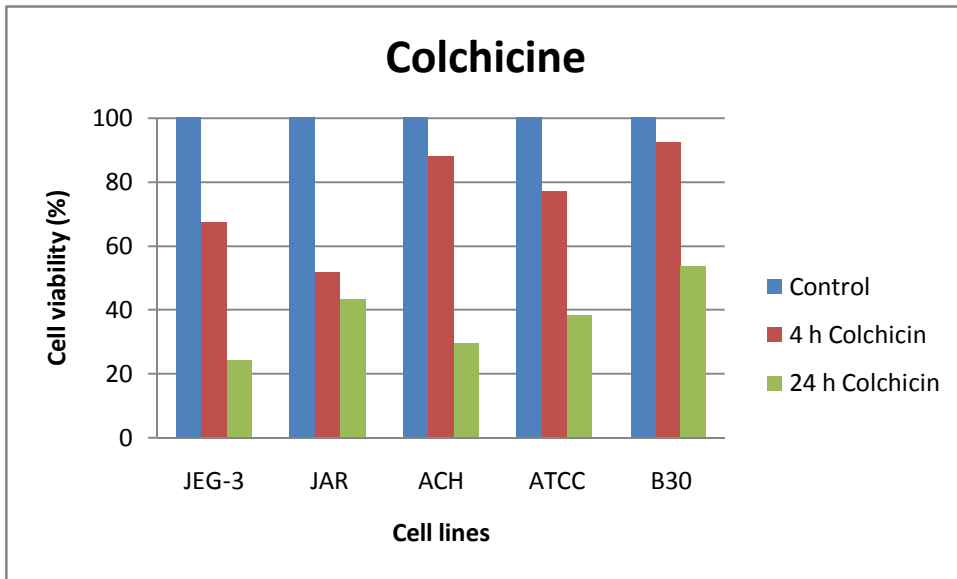


Figure 21.: Cell viability after 4 hours of colchicines exposure.

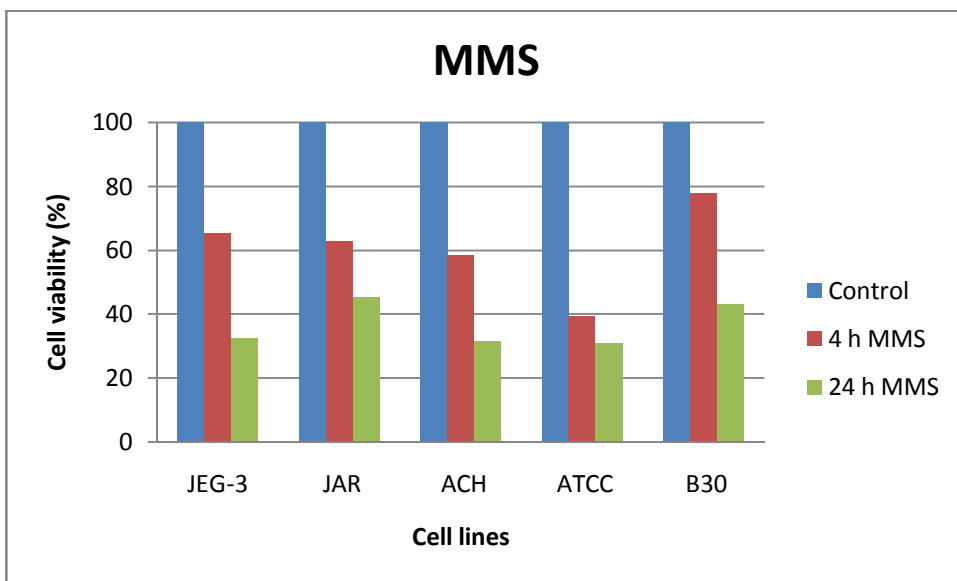


Figure 22.: Cell viability after 4 hours of MMS exposure.

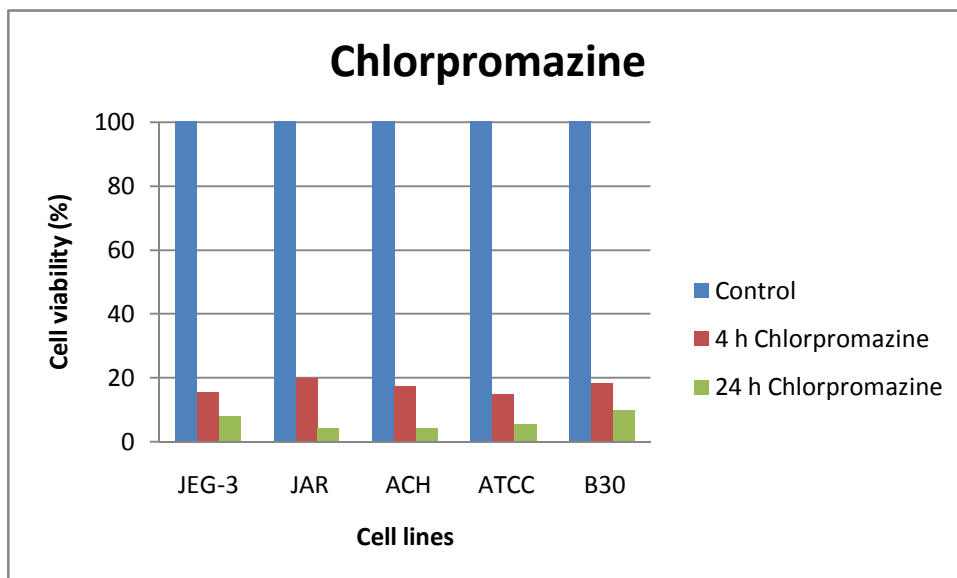


Figure 23.: Cell viability after 4 hours of chlorpromazine exposure.

The wells were seeded equally with 2.5×10^4 cells for each cell line. In order to reach a highly confluent layer, the cells were incubated for 24 hours at 37°C, 5% CO₂ environment. Fluorescence was measured by PrestoBlue, which was converted by mitochondrial enzymes of the viable cells. The reagent exhibits a change in color and shift can be detected in the fluorescence. To estimate the time dependence of this experiment, the percentages of living cells were determined after 4 and 24 hours of poison exposure (Figure 21, 22 and 23). Shorter exposure period were performed for subsequent experiments to allow for faster analyses. While all tested toxins reduced the metabolic activity of the cells, sensitivities to them varied. The lowest cytotoxicity was yielded to colchicin. Colchicin inhibits polymerization by binding to tubulin, one of the main constituents of microtubules. Availability of tubulin is essential to mitosis, so it effectively functions as a “mitotic” poison. After 4 hours of exposure, the BeWo cell lines showed high resistivity. These cell lines form a stable and confluent layer. While JAR reached EC₅₀, where 50% of the cells were non-living. The effect of MMS was more intense after the first measurement, since it stalls replication forks, and cells that are homologous recombination-deficient have difficulty repairing the damaged ones. Both colchicine and MMS cause cell damage, their affect after 24 hours of exposure can be considered similar toxic. The administration of chlorpromazine resulted in a significant reduction in the metabolic activity of the cells. The lowest cell viability was

obtained, since it inhibits cell proliferation, and decreases the rate of DNA synthesis. This effect induces irreversible changes the cells are not able to proliferate. Cell apoptosis was induced in a very short time independently from the structure and morphology of the cells.

As consequence, it can be stated, that all poisons showed cytotoxic effect, but the most sever was addressed to chlorpromazine. B30 was the most resistant against MMS and colchicine. The outcome of the comparative analysis showed that the cell lines, that were forming a monolayer were more resistant against each toxin, than the ones forming monolayer.

The next cytotoxicity measurement was focusing only on ATCC and B30 (Figure 24, 25). Both cell lines are derived from human choriocarcinoma. ATCC has a 3D structure, building a complex multilayer, while B30 forms monolayer during proliferation. This enables an interesting comparison of the effect of toxicity on diverse cell morphology. Different concentrations were used. Since the chlorpromazine was dissolved in sterile distilled water, vehicle was also measured. Water as medium induces stress to the cells, which can lead to cell apoptosis. Therefore it was inevitable to monitor, whether the different concentration of water has comparable negative effect on the cell viability, furthermore to be able to distinguish the toxicity of chlorpromazine. 4 hours of toxin exposure with different concentration was examined. B30 cell viability was reduced less than 10% after the treatment of 15.5, 32, 62 and 125 μM MMS (Figure 24). Cell viability showed highly similar values after the exposure of 250, 500 and 1000 μM MMS ($83\pm 6.4\%$, $84\pm 5.1\%$ and $81.9\pm 4.3\%$). The effect colchicine showed similar slight effect on the cells. 250 μM colchicine caused 15% cell apoptosis, 500 μM $16\pm 4.5\%$. Metabolic activity could be detected at $85\pm 6.8\%$ after the treatment of the highest dose. The treatment of different dose of colchicines showed a non-linear effect. On the other hand, the lowest dose of chlorpromazine induced a decrease in the viability by $30\pm 5.4\%$, 250 μM by $80\pm 6.3\%$ and 100% cell apoptosis was observed at the concentration of 1000 μM .

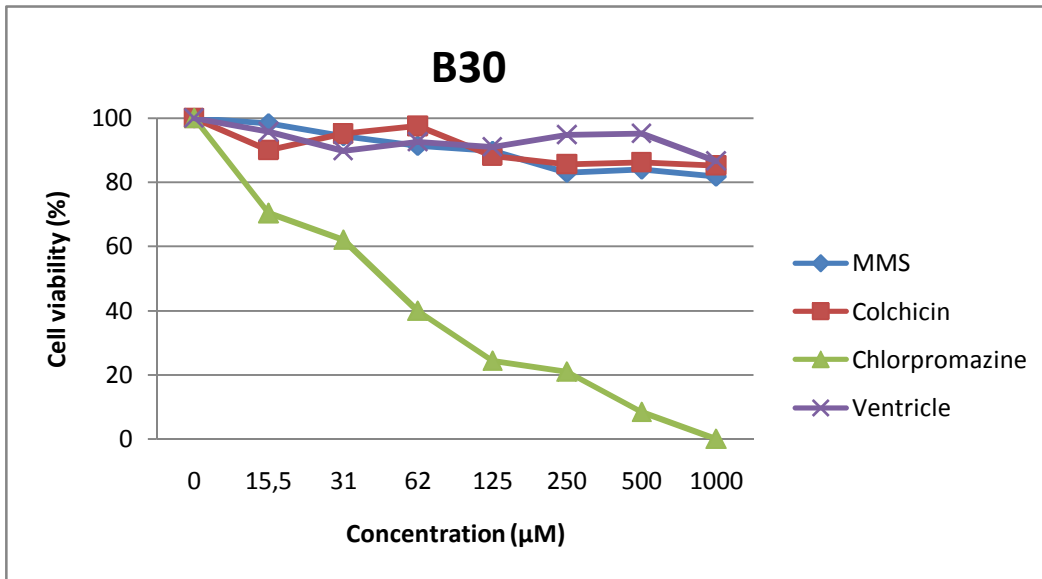


Figure 24.: B30 cell viability after exposure of toxins with different concentrations.

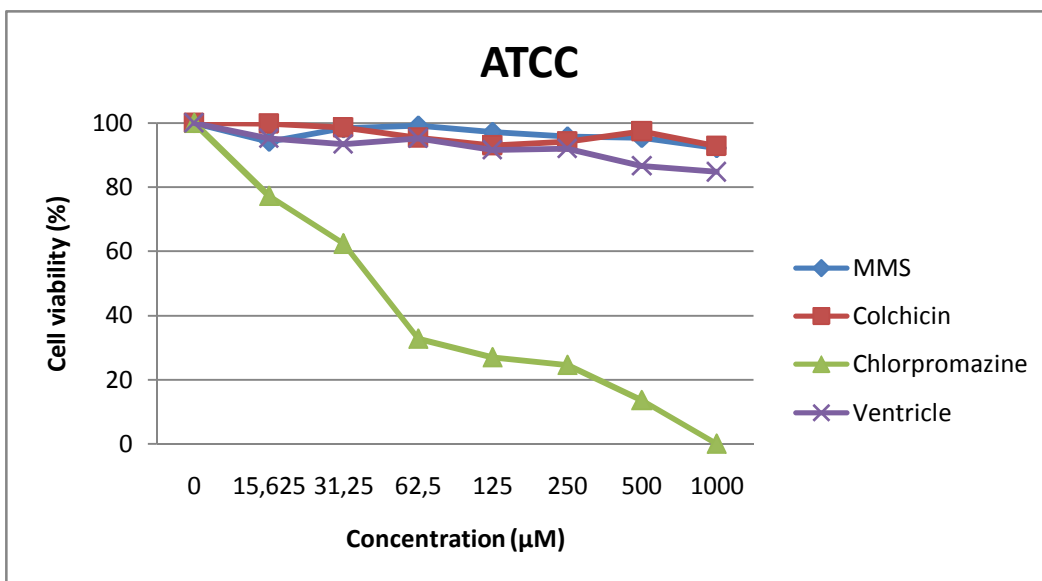


Figure 25.: ATCC cell viability after exposure of toxins with different concentrations.

Figure 25 showed that the lowest dose of colchicine that decreased the viability of ATCC cells was detected at 62.5 µM. The viability was reduced to 95±2.3%. Any significant reduction in the cell viability could not be observed after 4 hours. 125 µM exposure lead to 7.1±4.5% cell apoptosis, while a slight increase could be observed at the concentration of 250 and 500 µM. Cell viability was 94.1±3.5% at 250µM and 97.4±1.0% at 500 µM. 92.8±4.6% cell viability was yielded to the highest, 1000µM concentration. At the lowest MMS dose 5.8±3.5% cell apoptosis was obtained, while for 31, 62 and 125 µM these values were below 3±1.2%. 250

and 500 μM indicated $95\pm 2.0\%$ cell viability. Furthermore, the highest dose $92.1\pm 1.5\%$. The effect of chlorpromazine was more significant. Only the treatment of $15.62\mu\text{M}$ and $31\mu\text{M}$ yielded cell viability above EC_{50} ($72\pm 5.7\%$ and 628.2% , respectively.) $62.5\ \mu\text{M}$ chlorpromazine exposure resulted $67.4\pm 5.2\%$ cell death, $125\ \mu\text{M}$ $73.2\pm 4.6\%$ while $500\ \mu\text{M}$ $86.4\pm 7.1\%$. No living cell could be detected at $1000\ \mu\text{M}$.

These results demonstrate that all three toxins induced a time and dose-dependent decrease of impedance, indicating a global decline in cellular health after 4 hours. The effect of colchicines and MMS on both B30 and ATCC showed similarities. The applied concentrations ($15.5\text{-}1000\mu\text{M}$) did not affect cell viability significantly. The highest dose of MMS caused only 18.9% cell apoptosis, and colchicine 17.2% . The rate of non-living cells of ATCC was slightly higher. This can be explained by the morphology of the cell lines. B30 build a monolayer, the number of tight junctions are decreased compared to ATCC. Therefore ATCC cells form an expanded and complex layer, which is harder to penetrate by different toxins.

7.2.2. Cytotoxicity measurements of SiO_2 nanoparticles

Viability experiment with SiO_2 nanoparticles were carried out. Nanoparticles have medical use as anti-microbial agents, therapeutics, drug carriers and contrast agents. Due to the rapid increase of the usage of engineered nanomaterials, a reliable screening procedure is needed to identify the hazardous potential of these artificial nanomaterials. Before the exposure, in order to ensure the sterility of the NPs, they were filtered through a sterile filter with the pore size of $200\ \text{nm}$. The effect of the NPs was monitored in DMEM with 10% FCS serum, and without serum. Figure 26 show the cytotoxicity of the exposure after 4 hours. Vehicle was also measured in order to examine the effect of the medium and Presto Blue on the cells.

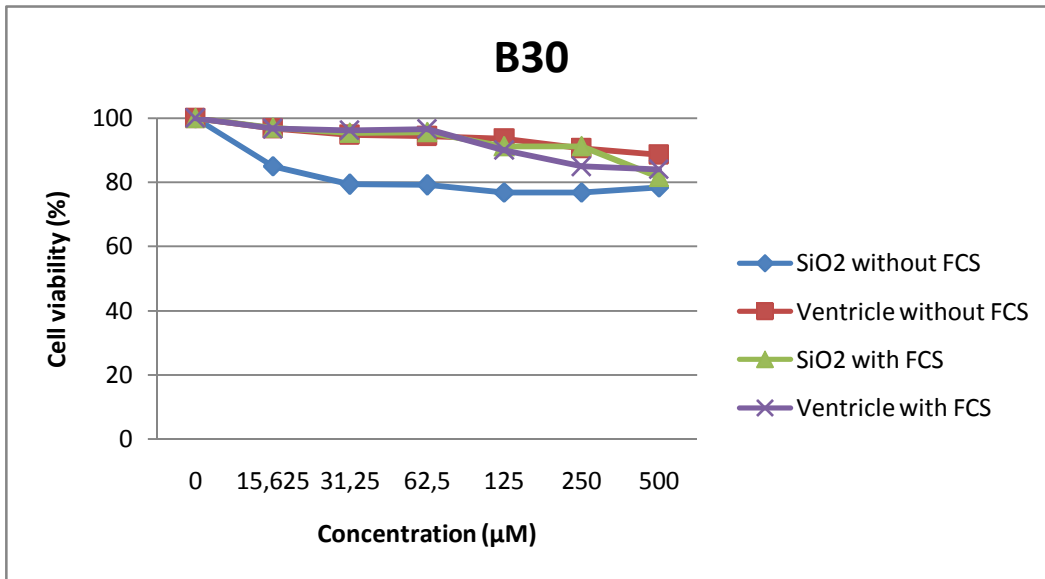


Figure 26.: B30 cell viability after 4 hours of exposure of SiO₂.

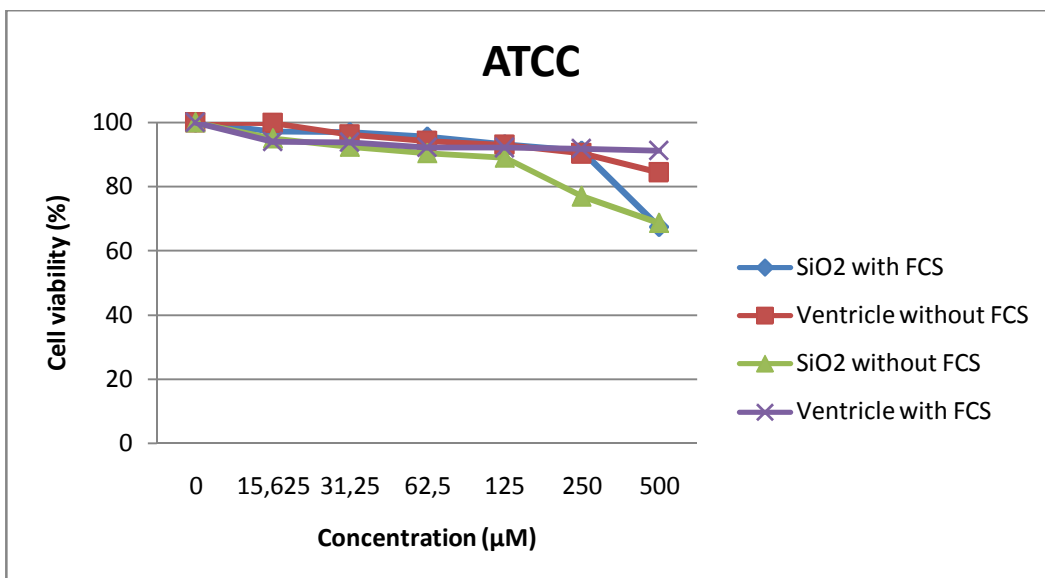


Figure 27.: ATCC cell viability after 4 hours of exposure of SiO₂

After the exposure of SiO₂ with FCS B30 viability was decreased by 3±1.2% at the dose of 15.625µM, by 4.6±2.3% at 31.25µM and by 4.4±1.9% at 62.5µM, respectively. The concentration of 125 and 250 µM reduced the viability by 8.9±3.4%. The highest dose, 500µM, resulted a viability rate of 81.9%. The viability was lower by the exposure of SiO₂ without FCS. 15.625µM caused 15±3.5% cell death, the following concentrations had similar effect on the cell viability, with the rate of 76-78%. ATCC cells showed high resistivity against

SiO₂ with FCS (Figure 27). The cell viability was above 90% for 15.625, 31.25, 62.6 and 125 μM. The highest dose caused 32.7±4.6% cell death. After the exposure of SiO₂ without serum, the cell viability was higher than 90% only for 15.625, 31.25 and 62.5 μM. The dose of 125μM resulted in 89.1±3.5% cell viability, 250μM in 76.9±4.1% and 500μM in 68.6±3.6%, respectively. Both for B30 and ATCC the percentage of the living cells are above 80%, during nanoparticle exposure with FCS. Significant difference can be observed between measurement with and without serum. The serum contains a complex array of protein components, which are essential to cell survival, growth and division. The protein corona building a homogen layer on the surface of the nanoparticles plays an important role in their interaction with living matter, reducing their cytotoxicity [63]. Therefore cells lack in FCS serum is less resistant against NPs. The cytotoxicity of the NPs also has a size-dependency. The smaller the particle is, the harmful for the cell, since smaller particles are able to penetrate the cell membrane [64]. Therefore the filtering process might also affect the cytotoxicity effect of the NPs on the cells. Even though the pore size of the filter was 200 nm, they could be sealed, as 1 ml NP solution with a pore size of 10-100 nm was flown through it. This could explain the low toxicity of the exposure.

7.3. Trans-epithelial endothelial resistance measurements

In this section, in order to carry out further analysis of the permeability properties of the different placenta cell lines transepithelial/endothelial electrical resistance measurement method was carried out. TEER has been the most commonly used parameter to evaluate the functionality of different barriers. Using TEER the characterization of permeability properties of placenta cells grown on permeable support establishes the basis for future application of this *in vitro* system to investigate transplacental transport and metabolism of drugs and drugs of abuse. Various TEER methods were used to evaluate the structural and functional properties of the placenta barrier. These methods included measurement of TEER according to different protocols and seeding densities, furthermore permeability measurements of various types and sizes of molecules through the barrier.

7.3.1. Characterization of TEER

TEER measurements are temperature-dependent; they are carried out ideally at constant temperature. Since the cells are incubated at 37°C and the assembly of the measurement poses some practical issues in the incubator, they have to be carried out at room temperature. The temperature fluctuation of the measurement method was monitored. Transwell was placed on a hot plate, the wells were filled with PBS. The resistance of the PBS solution was measured with EVOM2 VoltOhm Meter device at room temperature and at 37°C. The increase of the TEER values is shown in the graph below. To overcome the influence of the fluctuation of the temperature, before every TEER measurement, Transwell was placed in the laminar for 40 min to cool down and to carry out the measurements at room temperature.

Placenta cells have been subcultured and maintained in the T75 culture flasks. The cell seeding density was 10×10^5 /well. This density is optimal for reproducibly establishing cell monolayer cultures. Figure 28. shows the development of electrical resistance as a function of day in the culture postseeding. Triplicates were used for each cell type. TEER measurement for one cell line was carried out in two wells after medium change. The third well was measured also in fresh medium but after three washes of PBS. The normalized values are shown. Between the TEER values of the different measurement methods difference could be observed. The highest TEER measured in medium was yielded to JEG-3 with the value of $291 \pm 1.52 \Omega$, following by ACH of $278 \pm 1.52 \Omega$ on the last day. The impedance of ATCC increased to $165 \pm 1 \Omega$, B30 to $162 \pm 2 \Omega$. The lowest value but the most stable growth dynamics was yielded to JAR, $155 \pm 2.51 \Omega$. The highest value with PBS wash was yielded to ACH, $101 \pm 1.52 \Omega$, followed by ATCC with $85 \pm 3 \Omega$. After 5 days of co-culturing, TEER of JEG-3, JAR and B30 resulted in similar values: $50.5 \pm 1.52 \Omega$, $55 \pm 1.52 \Omega$, $60 \pm 2 \Omega$ respectively. The values for each cell type are significant higher in medium than those measured after PBS wash. This can be explained by the shear stress caused to the cells by the repeated washes. Stress can affect the barrier functions of endothelial cells and poorly adhered cells can be washed away from the membrane, therefore decreasing the TEER values of endothelial cells. The resultant placenta barrier-like cells possessed tight junctions and displayed intermediated TEER values ($167-291 \Omega$) measuring without PBS wash. JEG-3 resulted in highest values, which has the

shorter doubling time. The BeWo (ACH, ATCC and B30) cell lines show similar culturing and growing dynamics, as they form a confluent monolayer over the time. TEER measured after PBS wash shows significantly lower values (51-112Ω) JEG-3 and JAR cell line showed high values during the first three day of culturing, the monolayer became instable which resulted a decrease in TEER. The highest values were performed by BeWo cell lines: ACH $112 \pm 1.52 \Omega$, B30 $60.9 \pm 2 \Omega$. The PBS was did not cause a drop in TEER, the cell lines formed a stable, but poorly confluent layer. This method shows one limitation of TEER measurement, since the values highly depend on the handling. Due to the fluctuations of TEER values (Figure 28.) it is not possible to carry out repeatable and reliable measurement with washed of transwells.

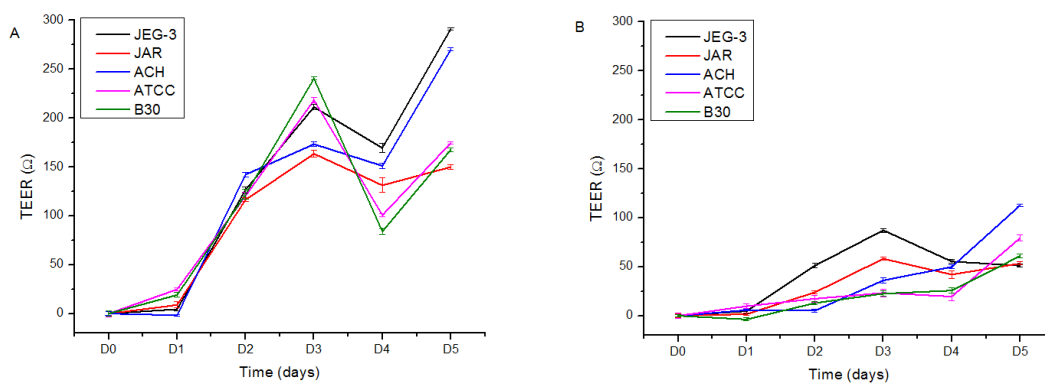


Figure 28.: TEER measurement without and with PBS wash.

7.3.2. TEER experiment with different seeding density

The previous experiment showed that a confluent monolayer can be formed with the seeding density of 10^5 cells/well. In order to avoid the stress on the cells, TEER measurement was repeated without PBS wash, medium was not changed after seeding. Importantly, TEER measurement depends not only on the temperature and stress applied to the cells but also on the seeding density. The density of placenta cultures during the differentiation process can significantly impact the differentiation yield, which can affect the degree of cell-cell contact. Lower cell number indicates slower/lower growth factor and lower TEER values. Figure x shows the TEER values with the seeding density of 10^5 , $5 \cdot 10^4$ and $2.5 \cdot 10^4$.

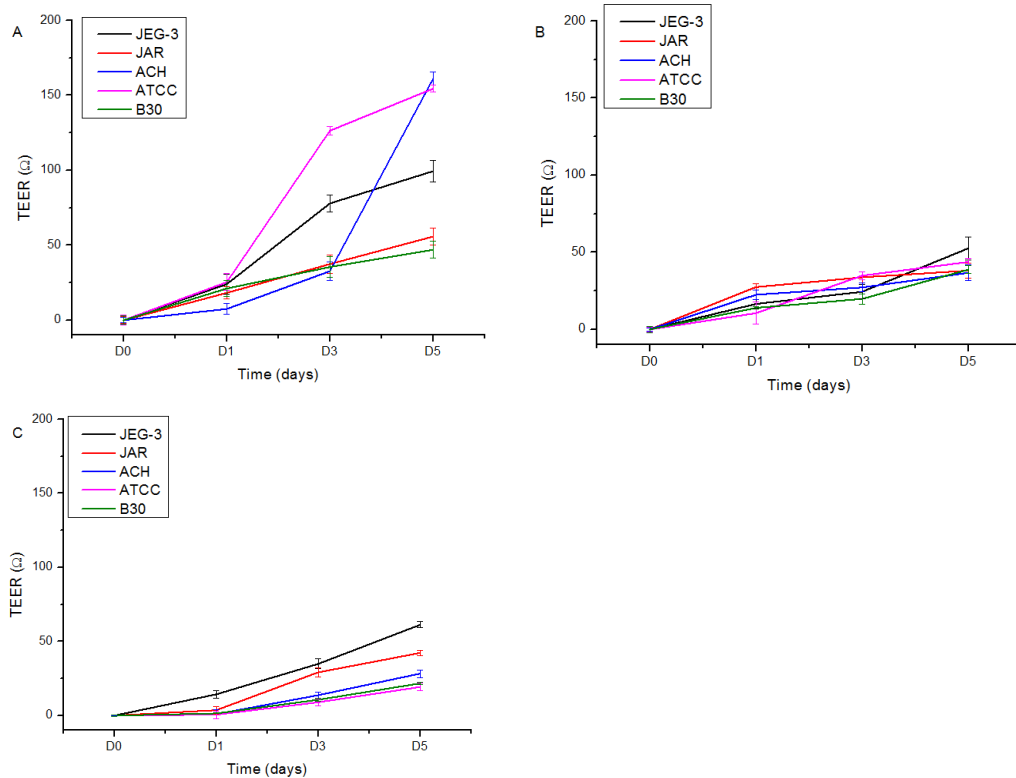


Figure 29.: TEER measurement with five placenta cell line with the seeding density of 10^5 (A), $5 \cdot 10^4$ (B) and $2.5 \cdot 10^4$ (C).

The highest seeding density resulted the highest TEER values. Stable and dynamic growth could be observed. The highest impedance was yielded to ATCC, $152 \pm 2.39 \Omega$ (Figure 29a). Until the 3rd day, the growth of ACH was the slowest, after the next 48 hours the impedance was increased by $125 \pm 4.35 \Omega$. JAR and B30 showed similar formation of monolayer, with the highest impedance of $51 \pm 5.8 \Omega$ and $48 \pm 5.6 \Omega$. $5 \cdot 10^4$ cell/well indicated lower impedance. On the 5th day a narrow spectrum of TEER was detected (Figure 29b). JEG-3 built the most confluent multilayer, with the value of $51 \pm 2.51 \Omega$, following by ATCC with $45 \pm 1.57 \Omega$. JAR, ACH and B30 formed a monolayer, resulting lower impedance: $36 \pm 2 \Omega$, $34 \pm 3.2 \Omega$ and $33 \pm 1.52 \Omega$, respectively. With the seeding density of $2.5 \cdot 10^4$ cells low TEER values was measured. The highest impedance was yielded to JEG-3, with $52 \pm 1.52 \Omega$.

At the seeding density of 10^5 and $5 \cdot 10^4$ can be seen, that the cells form a confluent layer between the 3rd and 5th layer, as they reach a plateau. The investigated placenta cell lines have different morphology, which indicated different characteristics. JEG-3 and ATCC cell lines are able to form a 3D structure during proliferation,

which indicate the high TEER values. In contrast to JAR, ACH and BeWo-B30, which are building significantly thinner monolayers. The seeding density of 2.5×10^4 cells shows poor TEER data (19-61 Ω), this short period of time was not sufficient to build a confluent layer (Figure 29c).

7.3.2. TEER permeability experiment

TEER permeability measurements were carried out with MMS, colchicine and chlorpromazine. The effect of the poisons was examined using the concentrations that have already been investigated during viability test. Only the results of ATCC and BeWo-b30 are shown, because BeWo cell lines are stable, grow to confluent layers and therefore they have been widely used by research groups.

At the highest seeding density of ATCC (Figure 30a), after 4 hours of MMS exposure, the initial TEER value was decreased from $105.6 \pm 7.62\Omega$ to $66.6 \pm 5.31\Omega$, after 24 hours this value was decreased to $50 \pm 2\Omega$. Colchicine reduced TEER to $72.6 \pm 2.5\Omega$ and after 24 hours to $47.3 \pm 4\Omega$. Chlorpromazine resulted in a more drastic effect, after 4 hours $10.1 \pm 4.2\Omega$ could be measured. After 24 hours 100% cell apoptosis was discovered. The effect of the toxins was similar on B30 cells (Figure 30b). MMS treatment caused a drop of 54% after 4 hours of exposure, and 100% cell apoptosis was detected after 24 hours. Colchicine decreased TEER by 61% (from $44.9 \pm 6.4\Omega$ to $17.8 \pm 5.2\Omega$) and after 24 hours TEER was $8.6 \pm 2.51\Omega$. After 4 hours of chlorpromazine treatment, 100% apoptosis was discovered. At the seeding density of 5×10^4 , TEER values of ATCC were decreased from $43.75 \pm 2.51\Omega$ to $32.7 \pm 1.02\Omega$ after 4 hours of MMS exposure and to $13.2 \pm 1.66\Omega$ after 24 hours (Figure 30c). Colchicine reduced TEER to $34.2 \pm 3.05\Omega$ and further to $14.5 \pm 2.51\Omega$ after 24 hours. Chlorpromazine induced a 60% drop after 4 hours and reduced the impedance further to 86% after 24 hours. The impedance of B30 cells after 4 hours of MMS treatment was decreased to $21 \pm 1.06\Omega$, after 24 hours this value was $10 \pm 2.3\Omega$. (Figure 30d) The treatment of colchicines resulted a drop of 5 Ω ($19 \pm 3.62\Omega$) after 4 hours and further decrease to $9 \pm 3.21\Omega$ was discovered. Chlorpromazine indicated a TEER value of $7\Omega \pm$ after 4 hours, and $3\Omega \pm 1.52\Omega$ after 24 hours. At the lowest seeding density of ATCC MMS and colchicine resulted in similar effects (Figure 30e). After 4 hours of exposure, TEER was decreased to $15.4 \pm 2.51\Omega$ measured in MMS and $13.8 \pm 1.05\Omega$ in

colchicine. After 24 hours the values were further reduced to $10.9 \pm 3.05 \Omega$ and $11.7 \Omega \pm 1.04 \Omega$, respectively. Chlorpromazine caused after 4 hours 100% cell apoptosis. The reaction toxins on B30 cells were the most significant (Figure 30f).

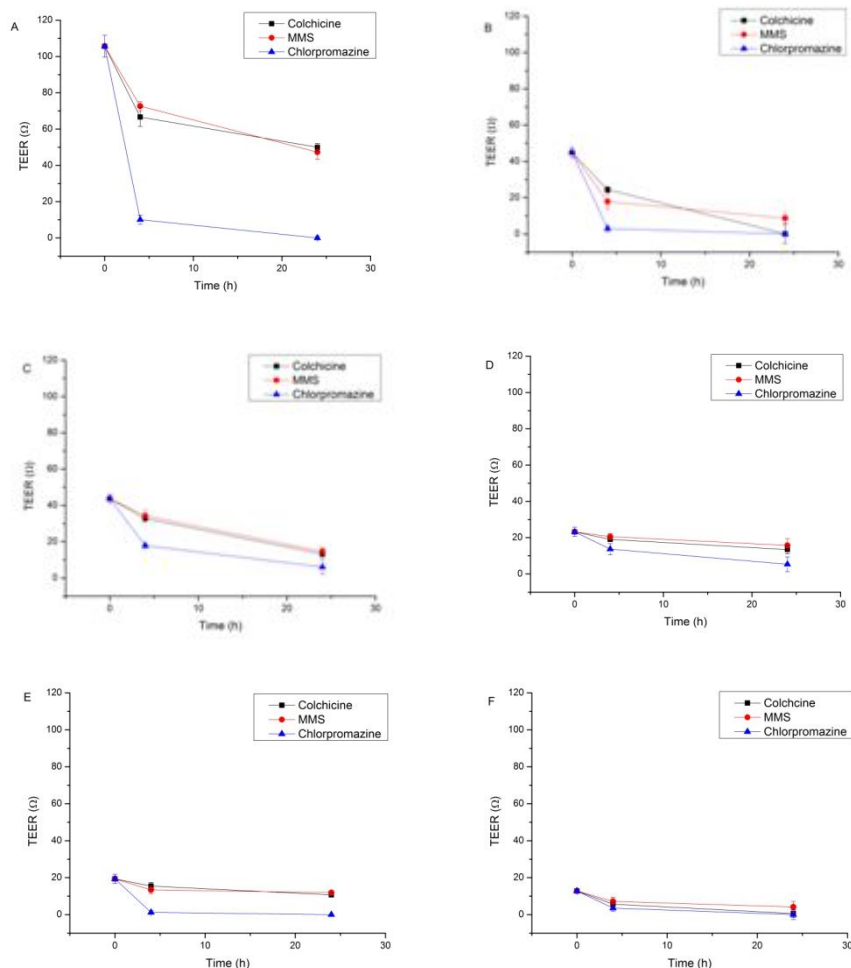


Figure 30.: The effect of colchicines, MMS and chlorpromazine on ATCC and B30 with different seeding densities: A. ATCC 10^5 cells/well, B. B30 10^5 cells/well, C. ATCC 5×10^4 cells/well, D. B30 5×10^4 cells/well, E. ATCC 2.5×10^4 cells/well, F B30 2.5×10^4 cells/well.

As it already has been discussed ATCC poses 3D structure, while BeWo-b30 2D. The difference enables the comparison of TEER values of cells with diverse morphology, since the TEER value of a multilayer is significantly higher than one of a monolayer. This difference could be observed at each seeding density.

The high TEER value of ATCC at the seeding density of 10^5 indicated a confluent and homogeny multilayer after 5 days of co-culturing. After 4 hours of MMS and colchicine a

decrease could be detected in the impedance. Colchicine disrupts the integrity and cell-matrix adhesion even by low-dose. The quality of tight junctions was decreased, the intercellular spaces were dilated. The cell enlarged, furthermore the tight junctions became permeable to colchicine. Similar effect could be discovered by B30, with the difference that the initial impedance was lower, since they form a monolayer. It can be stated, that the seeding density did not affect the results, when the cells are able to form a confluent layer. The effect of the chlorpromazine was detected as the strongest. This toxin destabilizes intercellular tight junctions via reactive oxygen species-mediated effects of TJ-associated F-actin distribution [65]. These changes cause cell apoptosis in a short period of time, independently of the quality of the multi- and monolayer. This can be seen on Figure 35. Already after 4 hours of exposure, both ATCC and B30 cells with different seeding density suffered apoptosis. The measured impedance of ATCC and B30 at the lowest cell density was slightly different. Here, the low number of cells could also influence negatively the TEER values, since the time was not sufficient to cell proliferation. For this density longer period of time might be needed to carry out a reliable measurement.

7.3.3. TEER permeability experiment on SiO₂ nanoparticle

The effect of SiO₂ nanoparticles was also monitored during TEER measurement to study the permeability of the tight junctions of the cells. After 5 days of co-culturing ATCC and B30 cells with the seeding density of 10⁵ cells, SiO₂ nanoparticles were administrated according to the concentrations described in Material and Methods. The effect of the NPs was monitored with and without FCS to evaluate the corona effect on the toxicity. The measured values are represented in the graphs below. The initial TEER value of B30 was 51±2.51Ω measured in medium with 10% FCS (Figure 31). A linear decrease in the impedance could be observed with increasing SiO₂ concentration. 31.25μM SiO₂ reduced the impedance only by 4±1Ω, while the concentration of 125μM by 10±1.05Ω. The highest dose led to a decrease of 17±2.51Ω. The values measured in the absence of FCS serum were significantly lower. While the impedance was 40.5±4.05Ω at the concentration of 31.25μM, at 125μM only 17±Ω could be measured. The TEER values of ATCC were also reduced after the exposure of NPs (Figure 32). TEER values after treatment of SiO₂ with FCS did not change drastically independently

the concentrations. TEER without any NP was $141 \pm 5.65 \Omega$, while with $500 \mu\text{M}$ was $128 \pm 3.52 \Omega$. Furthermore, after the exposure of 0 - $125 \mu\text{M}$ SiO_2 without FCS, TEER values were between $134 \pm 4.05 \Omega$ and $119.5 \pm 3.21 \Omega$. The impedance was reduced to $90 \pm 4.04 \Omega$ at the concentration of $250 \mu\text{M}$, and to $77.5 \pm 1.05 \Omega$ at $500 \mu\text{M}$.

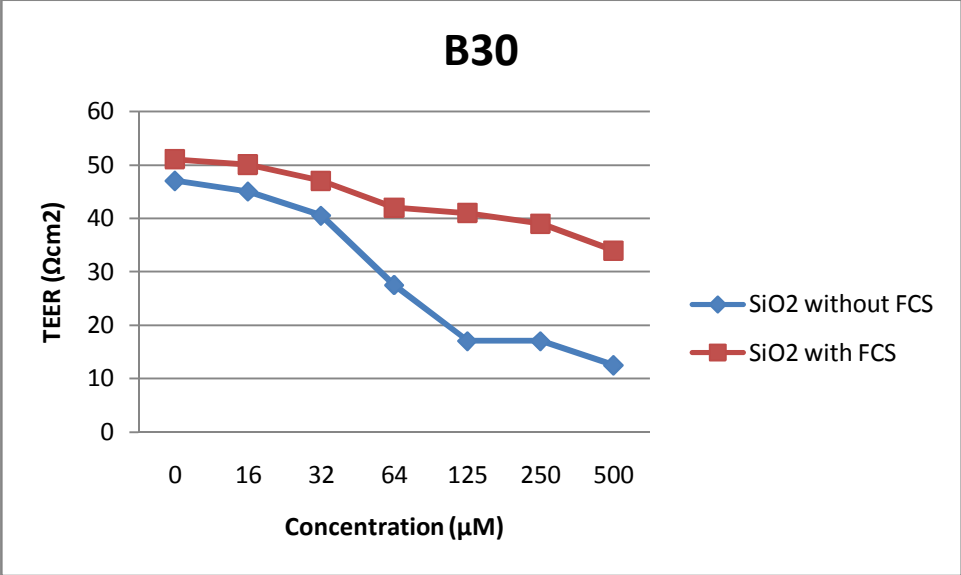


Figure 31.: B30 TEER measurement after 4 hours of SiO_2 exposure

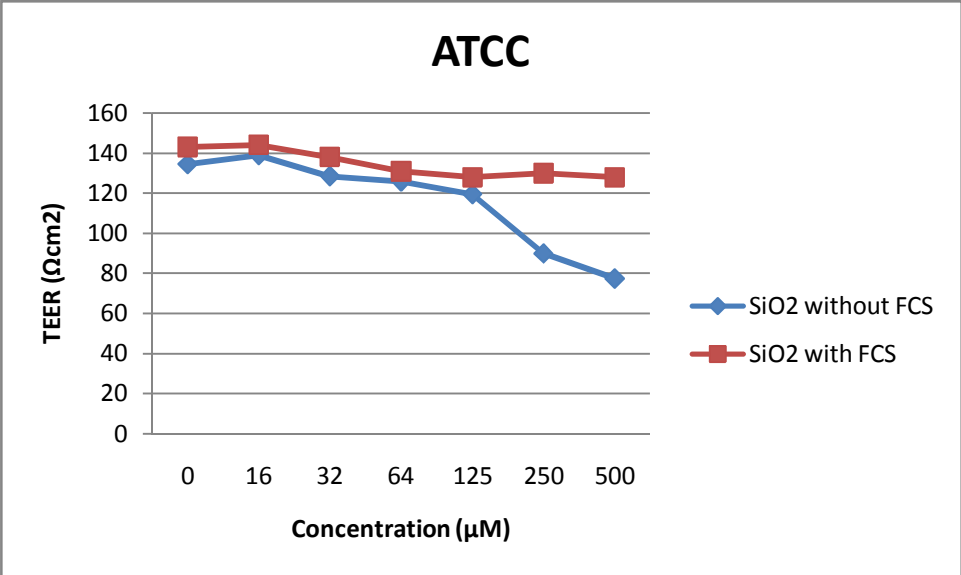


Figure 32.: ATCC TEER measurement after 4 hours of SiO_2 exposure

As it can be seen Figure 31, B30 cells were dose-sensitive to NP exposure. The decreasing TEER values indicate that as B30 cells form a confluent monolayer, the tight junctions can already be disrupted by low-dose exposure. The cell membrane became leaky, and NPs were able to penetrate the cell. The values measured in medium with FCS serum are higher, as the protein built a homogen layer around the NPs, reducing their toxicity. ATCC cell was more resistant against the NPs, which can be explained by the higher TEER values. During the measurement with FCS, the impedance values indicated, that the cells formed a confluent multilayer with tight junctions, furthermore due to the corona effect, the toxicity of the SiO₂ was reduced.

7.4. Electrical impedance spectroscopy measurements

In this chapter impedance measurement will be discussed. This method enables to carry out a continuous, long-time measurement. Here not only and the formation of tight junctions between the cells can be monitored, but also the analysis of the cell adhesion, cell-surface attachment. The measurements were carried out on a chip under static and dynamic conditions. The goal of the experiment was to develop a platform for impedance measurement to get an insight into dose-dependent disruption of intercellular and cell-substrate adhesion due to toxins (colchicine, chlorpromazine, MMS) and SiO₂ nanoparticles.

7.4. 1. Electrode characterization for electrical cell-substrate impedance sensing

First, characterization of chip and measurement method was done. This process was inevitable in order to carry out a reliable, reproducible measurement under suitable conditions for the cells. A glass surface with microfluidic channel (blank chip) was developed in order to find a channel design to monitor the adhesion process of the cells. This design also needs to ensure a bubble-free environment for the cells, since it is inevitable for microfluidic measurements.

7.4.1.1. Cell adhesion on blank chip

A microfluidic channel system was built between two glass surfaces as described in Materials and Methods sections. This blank chip was placed on a pre-heated surface of 37°C. The

temperature of the plate was monitored by a PT100 sensor fixed on the surface and measured with multimeter. The values were between 114.2-114.8 Ω , the resistance converted to temperature is 36.8-37.2°C. For this experiment ACH-3P placenta cell line was used, 1ml medium with 10^6 cells were injected into the channel. The surface of the channel, where the cells are able to adhere is 40 mm².

Before the injection of the cell the flow was stopped. The adhesion process was monitored. Images were taken by microscope at 0, 4 and 20 hours after cell seeding. As Figure 33 shows the changes in the cell morphology during cell adhesion can be observed already after 2 hours of seeding. After 20 hours, the cells form tight junctions and small islands are visible. This indicates that for cell adhesion, the design ensured a suitable and sterile environment.



Figure 33.: Cell adhesion mechanism

7.4.1. 2. Formation of air bubbles in chip

During microfluidic experiments, it is inevitable to avoid gas bubbles in the system. First, they interrupt the desired circulation of the fluid and furthermore are able to damage the cells at the interface of the liquid-gas bubbles. Bubbles are cytotoxic to mammalian cells, due to the high surface tension of the air-liquid interface which is able to rupture the cell membrane [66]. Formation and accumulation of air bubble is especially in a long-term cell culture is critical. Occasionally and continuously arise of bubbles are due to factors like changes in temperature, channel geometry, hydrophobic properties of PDMS, configurations of connectors and valves [67]. In order to succeed a bubble-free environment, the chip was placed on a heated surface, with the temperature of 37°C, and pre-heated medium was used. The fist chip design was 70 μm high. Even though the cell injection was carry out without air bubble, due to the static flow conditions, air diffused into the channel through

the outlet pipe. To overcome this issue, a chip with greater channel high was developed, with the height of 210 μm . The design offered a greater volume, but during 6 hours adsorption time, the problem of gas-bubble formation could not be solved. It can be explained, that the adhesive layers did not stick flawlessly to each other. This led to the next chip design attempt, which was built with PDMS instead of adhesive tape.



Figure 34.: Air bubble formation over the time with the different chip design.

7.4.1. 3. PDMS characterization for chip

PDMS has naturally a hydrophobic surface due to the repeating units of $-\text{O}-\text{Si}(\text{CH}_3)_2$ -groups. Exposure to plasma destroys methyl groups ($\text{Si}-\text{CH}_3$) by introducing silanol groups ($\text{Si}-\text{OH}$) making the surface hydrophilic. [68] Due to its hydrophilic nature, furthermore to its low costs and easy handling properties it is favorable to use PDMS for microfluidic devices. Plasma treatment is a very effective method to clean, sterilize and activate the surface of substrates such as glass and PDMS in order to perform an irreversible bonding process. The cleaning and activating process of the surface of the biochip is performed with plasma treatment. In order to avoid the damage of electrodes characterization of the plasma treatment method is necessary (Figure 35).



Figure 35.: Not suitable period of time and power of plasma exposure lead to delamination of the electrode.

The results were graded from 1 to 5, where 1 means, that the adhesion was poor, PDMS could be removed from the glass easily. 5 means that the bonding process was performed perfectly, PDMS could not be removed from the glass by pulling with tweezers.

Time (min:sec)	Intensity of the plasma					
	High		Medium		Low	
	1st day	2nd day	1st day	2nd day	1st day	2nd day
2:00	5	5	5	5	4	4
1:30	3	5	3	4	3	3
1:00	3	4	3	4	5	5
0:30	4	4	2	3	3	5
0:15	2	4	4	5	3	3
0:05	2	2	3	5	4	4

Figure 36.: Grading: 5: very good adhesion, 1: very bad adhesion

As it is showed in the table above, experiments were carried out with different duration and power of plasma exposure. Also the endurance of the bonding was studied after 24 hours of the plasma treatment. The quality of the bonding is significantly more dependent and sensitive on the duration of the exposure than on the power.

As conclusion, in order to prevent the electrodes of any damage that can be caused by plasma treatment, it is necessary to set lower intensity. To increase the quality of the bonding, it is recommended to leave the bonded parts overnight and press together with additional pliers.

7.4.2. Characterization of EIS measurement with physiological buffer

First a commonly used physiological buffer (PBS- phosphate buffered saline) solution with the same osmolarity and pH as the cell culture medium was used as reference electrolyte. The solution with different concentrations was applied to the gold electrodes. After a stable baseline was detected, PBS solution with different concentrations was injected into the channel, starting with the lowest (Figure 37). Here, the effect of ionic concentration change can be studied. The highest impedance (245 Ω) was observed at the lowest PBS concentration (0.3125mM). 0.625mM PBS solution resulted a decrease of 65 Ω in the impedance. 1.25mM solution had an impedance value of 98 Ω . 2.5 mM concentration decreased the impedance to 61 Ω . Furthermore the PBS solution with 5mM resulted 36 Ω and 10mM 24 Ω , respectively.

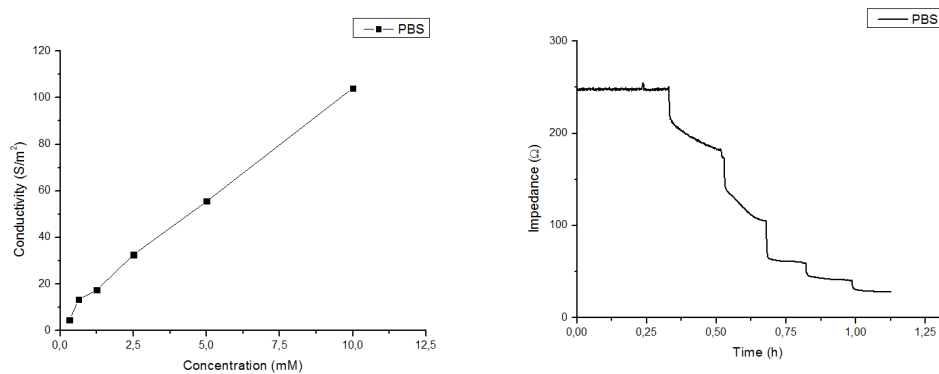


Figure 37: The conductivity of the applied PBS concentrations can be seen on figure a. Figure b shows the impedance of the solutions with increasing concentrations.

PBS concentrations of 2.5, 5 and 10mM resulted in a significant stable impedance value, and indicated lower decrease.

7.4.3. Impedance spectroscopy measurement to monitor cell adhesion

Electrical impedance spectroscopy was carried out with electrode embedded in the chip. The cell adherence inspection on all chips shows no difference compared to that in the culture flask and blank chips. The impedance value of the MEM-based medium measured with the Au sensor was between 140-250Ω. Potentiostat was used for impedance measurement. The signal amplitude of the externally applied sinus signal was set to 10 mV and the recorded value was averaged over 2 measurements per frequency. Six sinusoidal excitation frequencies of 10, 15, 22, 35, 53 and 80 kHz were traced. Over a total measurement each 15 seconds a measurement point was recorded. The cell chips were heated at 37°C. In the impedance diagrams displayed below only the results for a 10 kHz excitation signal are presented as they showed the maximal sensitivity.

Characterization of adhesion time and flow rate was carried out, in order to find the suitable setup for cell adhesion, furthermore cytotoxicity measurements. JEG-3 cells were used, because of their rapid proliferation. Although the geometry of the sensors was the same and the surface was pre-treated the same way, the impedance of the individual sensors is highly varying among each other. Optical investigations showed, that no visible disruption could be observed. Cell measurements were carried out with 4 and 8 μl/min flow rate, with the

adhesions time of 4 and 14 hours (Figure 38). 10^6 cells in 1 ml medium were injected into the system, and cell adhesion was observed under static conditions.

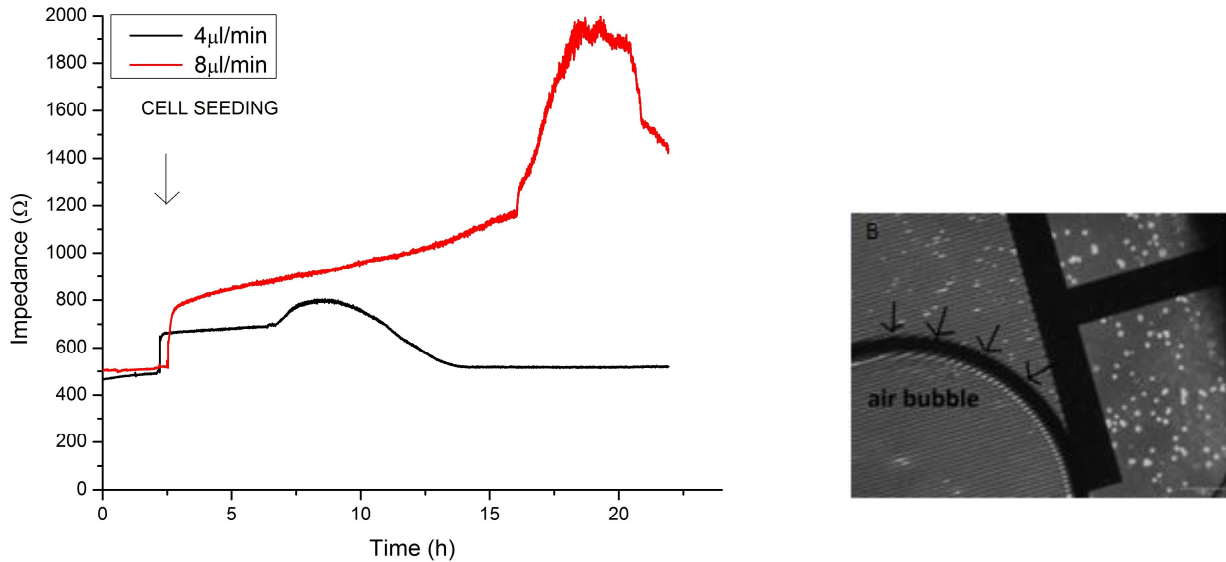


Figure 38.: After cell adhesion, the effect of an air bubble can be observed. In the case of $4\mu\text{l}/\text{min}$ flow rate, the air caused cell death, as the impedance decreased to the initial value.

At the measurement with the flow rate of $4\mu\text{l}/\text{min}$ increase in the impedance with 175Ω could be observed. At the flow rate of $8\mu\text{l}/\text{min}$ this value was 312Ω . After 14 hours the medium perfusion was started, continuous but drastic increase of the impedance with the value of 1000Ω could be observed, which can be yielded to air-bubble. In order to carry out a repeatable and reliable cell measurement, the system has to be sterile and air-bubble free during the whole experiment (Figure 38b). These issues led to a new electrode design, where the channel volume was increased. Instead of a PDMS layer with the thickness of $250\mu\text{m}$, one with 3mm was used.

7.4.4. Toxicity measurement of ATCC and B30 cells during impedance spectroscopy

Real-time impedance biosensing was carried out on B30 and ATCC cells. These two cell lines were chosen due to their high stability, growing into confluent mono- and multilayer. Moreover, these cell lines enable a comparison of the results of the cell adhesion and cytotoxicity measurement carried out with a commercially available TEER device.

Furthermore, toxicity of MMS was monitored using the same concentration as in TEER. During this experiment cells and microelectrodes could be combined in order to get an insight into dose-dependent disruption of intercellular and cell-substrate adhesion. Base line of DMEM+ was established (380Ω for sensor 1, 325Ω for sensor 2 and 302Ω for sensor 3) (Figure 39). Although the geometry of the sensors was the same and the surface was pre-treated the same way, the impedance of the individual sensors is highly varying among each other. Optical investigations showed, that no visible disruption could be observed. B30 cells are seeded at high density, 10^6 in 1 ml, on microelectrode arrays. After 14 hours of cell adhesion under static flow, medium perfusion was started through the channels. The increase of the impedance on sensor 1 resulted in 190Ω , on sensor 2 187Ω and on sensor 3 162Ω . The injection of MMS decreased the impedance values, after 24 hours the cells were washed out from the surface of the electrodes.

Sensor 1 was used to monitor the cell adhesion process without any toxin. The cells were adhered on the surface, leading to steady but significant increase in the impedance until reaching plateau. Small peaks could be observed in the graphs which indicate the pressure changes in the channels as the medium was started to perfuse.

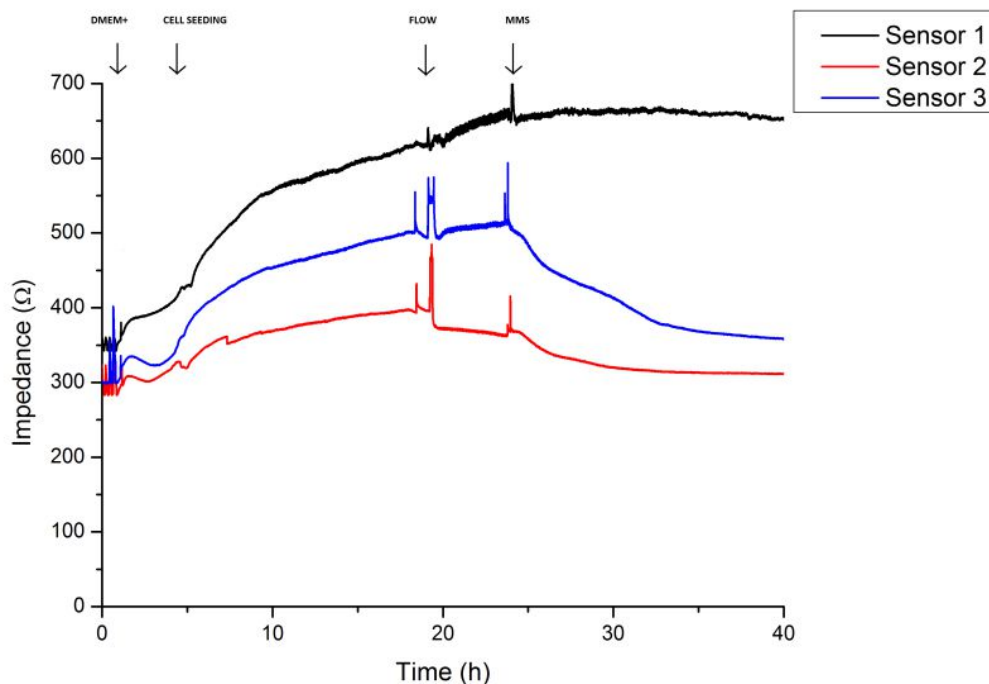


Figure 39.: Real-time impedance measurement of B30 cells. After 24 hours, MMS was introduced to the channel.

The effect of MMS was monitored on sensor 2 and 3 MMS exposure led to a decrease of the impedance, indicating a global decline in cell health. After 24 hours, the impedance reached the initial value, the cells were washed away from the surface of the electrode. The toxicity effect was stronger, than observed in TEER. This can be explained, that during this experiment continuous medium flow induced shear stress to the cells, which could not be observed during static conditions. The result of ATCC cytotoxicity measurement is not shown, since the adhesion of the cells and the cytotoxicity could not be observed. This also explains the fact, that B30 is the most stable placenta cell line used by research groups.

The effect of chlorpromazine on the adherent cells could not be examined, because the toxin led to electrode delamination (Figure 40).

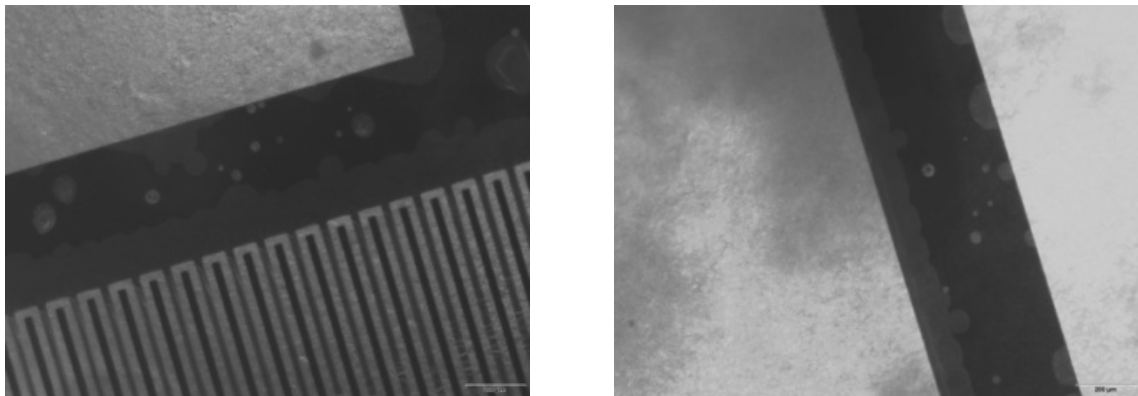


Figure 40.: Electrode delamination due to chlorpromazine. This issue not only resulted in a failure of impedance measurement but also lead to cell death.

8. Summary and Outlook

In this work, two impedance measurement methods were characterized and monitored in order to examine the quality of the barrier integrity of five placenta cell lines. First transepithelial endothelial electric resistance measurements were carried out. In this section the barrier properties of placenta cells were compared with a commercially available apparatus. It was demonstrated, that temperature fluctuation, different cell lines and number of the cells have a great impact on the barrier properties. Further measurements were carried out only with two placenta cell lines, ATCC and B30. ATCC forms confluent multilayer, B30 monolayer over the time, which enables the comparison of impedance measurements on cells with different morphology. The delivered results were used as reference for the further cytotoxicity measurements, where the effect of three substances (colchicine, chlorpromazine and methanemetanosulfate (MMS)) and Silica nanoparticle on the placenta barrier was examined. Time- and dose-dependent impact was observed. The impedance decreases with increasing concentrations of the toxins and with longer exposure time. This rate depends on the quality of the confluent layer and on the toxicity of the substances. ATCC was more resistance against the exposure, since it has a 3D cell layer structure. As the second part of the work, an in-built impedance spectroscopy platform was used. After the development a suitable biochip continuous measurement of cell adhesion was carried out in a wide frequency range. Real-time impedance sensing can give a better insight about the cell health and the induced disruptions in tight junctions and cell-surface adhesion. Since the transfer from static cell culture conditions to a microfluidic dynamic system a negative impact was resulted on the ATCC cell, cytotoxicity measurements were carried out only on B30 cell line.

The results of the cytotoxicity measurements both with static and dynamic systems proved that the placenta-barrier does not work as an impenetrable shell between the mother and fetus. This indicates that further investigations are required to improve the safety of the baby during the gestation.

To enable future impedance sensing measurements on different microelectrodes, new chip design and considerations will have to be adapted. These enable a transfer for the cells from static to dynamic condition and are resistant against the different substances. The

measurement will allow gaining a better insight into the underlying mechanism of a wide spectrum of chemical exposures and extending the capabilities of the discussed measurement method.

9. References

1. Gendron, *Health care providers' requests to Teratogen Information Services on medication use during pregnancy and lactation*. Eur J Clin Pharmacol, 2009.
2. Lupattelli, *Medication use in pregnancy: a cross-sectional, multinational web-based study*. BMJ Open, 2016.
3. Kim, *Thalidomide: The Tragedy of Birth Defects and the Effective Treatment of Disease*. Toxicological Sciences, 2011.
4. Brent, R., *Environmental causes of human congenital malformations the pediatrician's role in dealing with these complex clinical problems caused by a multiplicity of environmental and genetic factors*. Pediatrics, 2004.
5. Dreyer, N., *Direct-to-patient research: pilot a new approach to understanding drug safety during pregnancy*. JMIR Public Health Surveill, 2015.
6. Lee, J., *Placenta-on-a-chip: a novel platform to study the biology of the human placenta*. Journal of maternal-fetal and neonatal medicine, 2015.
7. Larsen, W., *Human Embryology: 3rd (third) Edition*. Elsevier Health Sciences 2002.
8. Cross, J.C., *Chorioallantoic morphogenesis and formation of the placental villous tree*. Ann N Y Acad Sci, 2003.
9. Watson, E.D., *Development of Structures and Transport Functions in the Mouse placenta*. Physiology, 2005.
10. Rosson, J., *Placental development: lessons from mouse mutants*. Nature, 2001.
11. Wang, Y., *Vascular Biology of the Placenta*. Morgan & Claypool Life Sciences, 2010.
12. Russel, G.M., *Mechanisms of drug transfer across the human placenta*. Pharmacy World and Science, 1998.
13. Gude, N.M., *Growth and function of the normal human placenta*. Thrombosis Research, 2004.
14. Smith, C., *Nutrient transport across the epithelium of the placenta*. Annu Rev Nutr, 1992.
15. Ahokas, R.A., *Development and Physiology of the Placenta and Membranes*. Glob. libr. women's med., 2008.
16. Jasson, T., *Amino Acid Transporters in the Human Placenta*. PEDIATRIC RESEARCH, 2001.
17. May, K., *Antibody-Dependent Transplacental Transfer of Malaria Blood-Stage Antigen Using a Human Ex Vivo Placental Perfusion Model*. PLoS One, 2009.
18. Levkovitz, R., *In vitro stimulation of placental transport: Part 1. Biological model of the placental barrier*. Placenta Journal, 2013.
19. Sastry, B., *Techniques to study human placental transport*. Adv Drug Deliv Rev, 1999.
20. Benirschke, K., *Pathology of the human placenta 5th edition*. Springer, 2006.
21. PL, G., *Animal models to study placental development and function throughout normal and dysfunctional human pregnancy*. Semin Reprod Med., 2016.
22. Bode, C.J., *In Vitro Models for Studying Trophoblast Transcellular Transport*. Methods Mol Med., 2006.

23. Fei, L., *Permeability properties of monolayers of the human trophoblast cell line BeWo*. Americal Physiological Society, 1997.
24. Avery, M.L., *The presence of inducible cytochrome P450 types 1A1 and 1A2 in the BeWo cell line*. Planceta 2003.
25. Lee, S., *Placenta-on-a-chip: a novel platform to study the biology of the human placenta*. J Matern Fetal Neonatal Med, 2016.
26. Wang, S., *Evaluation of Miniaturized Mixer and Integrated Optical Components for Cell Sorting* Master Thesis, 2008.
27. Park, E.S., *Continuously perfused, non-cross-contaminating microfluidic chamber array for studying cellular responses to orthogonal combinations of matrix and soluble signals*. Lab on a Chip, 2017.
28. Ye, N., *Cell-based high content screening using an integrated microfluidic device*. Lab Chip, 2007.
29. Zheng, X., *Cell-based biosensors: Towards the development of cellular monitoring*. Chinese Science Bulletin, 2002.
30. Mohanty, S.P., *Biosensors: A Tutorial review*. IEEE Potentials, 2006.
31. Skrádal, P., *Piezoelectric biosensors*. Trends in Analitical Chemistry, 2016.
32. Dixon, M., *QCM D monitoring: enabling real-time characterization of biological materials and their interactions* J Biomol Tech, 2008.
33. Megens, M., *Magnetic biochips: a newoption for sensitive diagnostics*. Journal of Magnetism and Magnetic Materials, 2005.
34. Graham, D., *Magnetoresistive-based biosensors and biochips*. Trends Biotechnol., 2004.
35. Ferreira, H.A., *Magnetosensitive dna chips based on ac field focusing of magnetics labels*. Journal of Applied Physics, 2006.
36. Goloverda, G., *Synthesis of ultrasmall magnetic iron oxide nanoparticles and study of their colloid and surface chemistry*. J Magn Magn Mater, 2009.
37. Llandro, J., *Magnetic biosensor technologies for medical applications a review*. Med Biol Eng Comput, 2010.
38. Schöning, M.J., *Recent advances in biologically sensitive field-effect transistors*. The Analyst, 2002.
39. Schoning, M.J.P., A., *Bio feds (field-effect devices): State-of-the-art and new directions*. Electroanalysis, 2006.
40. Bathia, S., *Microfluidic organs-on-chips*. Nature Biotechnology, 2014.
41. Srinivasan, B., *TEER measurement techniques for in vitro barrier model systems*. J Lab Autom., 2015.
42. Booth, R., *Characterization of a microfluidic in vitro model of the blood-brain barrier (μ BBB)*. Lab. Chip, 2012.
43. Mahler, G., *Characterization of a Gastrointestinal Tract Microscale Cell Culture Analog Used to Predict Drug Toxicity*. Biotechnol Bioeng., 2009.
44. Ingber, D.E., *Gut-on-a-Chip microenvironment induces human intestinal cells to undergo villus differentiation*. Integr Biol (Camb). 2013.
45. Huh, D., *Reconstituting Organ-Level Lung functions on a chip*. Science, 2010.
46. Knowlton, S., *A bioprinted liver-on-a-chip for drug screening applications*. Trends in Biotechnology, 2016.
47. Huh, D., *A microphysiological model of the human placental barrier*. Lab Chip, 2016.
48. Srinivasan, B., *TEER measurement techniques for in vitro barrier model systems*. J Lab Autom, 2015.
49. Lippmann, E.S., *Human Blood-Brain Barrier Endothelial Cells Derived from Pluripotent Stem Cells*. Nat Biotechnol., 2013.
50. Harrington, H., *Immunocompetent 3D Model of Human Upper Airway for Disease Modeling and In Vitro Drug Evaluation*. Mol Pharm, 2014.

51. Chen, S., *TEER: a functional parameter to monitor the quality of oviduct epithelial cells cultured on filter supports*. Histochem Cell Biol., 2015.
52. Montal, M., *Formation of biomolecular membranes from lipid monolayers and a study of their electrical properties*. Proc Natl Acad Sci U S A, 1972.
53. Ferrario, A., *Electrochemical impedance spectroscopy study of the cells adhesion over microelectrodes array*. 2011 7th Conference on Ph.D. Research in Microelectronics and Electronics, 2011.
54. Moore, E., *Monitoring of cell growth in vitro using biochips packaged with indium tin oxide sensors*. Sensors and Actuators B: Chemical, 2009.
55. Dean, D., *Electrical impedance spectroscopy study of biological tissues*. J Electrostat. , 2008.
56. Benson, K., *Impedance-based cell monitoring: barrier properties and beyond*. Fluids Barriers CNS, 2013.
57. Manual, W.P., *Instruction Manual EVOM2 Epithelial Voltohmmeter*. Instruction Manual.
58. Metrohm-Autolab, *Basic overview of the working principle of a potentiostat/galvanostat (PGSTAT) – Electrochemical cell setup.*. Autolab Application Manual.
59. Wadsack, C., *Trophoblast-like human choriocarcinoma cells serve as a suitable in vitro model for selective cholesteryl ester uptake from high density lipoproteins*. Eur J Biochem, 2003.
60. Grümmer, R., *Adhesion and Invasion of Three Human Choriocarcinoma Cell Lines into Human Endometrium in a Three-dimensional Organ Culture System*. Placenta Journal, 1994.
61. Hiden, U., *The first trimester human trophoblast cell line ACH-3P: a novel tool to study autocrine/paracrine regulatory loops of human trophoblast subpopulations--TNF-alpha stimulates MMP15 expression*. BMC Dev Biol., 2007.
62. Mauschitz, R., *Self-regulation of the endothelin receptor system in choriocarcinoma cells*. Biochimica et Biophysica Acta (BBA) - Molecular Basis of Disease, 2000.
63. Pino, P., *Protein corona formation around nanoparticles – from the past to the future*. Materials Horizons, 2014.
64. Huang, J.P., *Nanoparticles can cross mouse placenta and induce trophoblast apoptosis*. Placenta Journal, 2015.
65. Gamal, W., *Low-dose acetaminophen induces early disruption of cell-cell tight junctions in human hepatic cells and mouse liver*. Nature, 2017.
66. Kang, E., *A hemispherical microfluidic channel for the trapping and passive dissipation of microbubbles*. Journal of Micromechanics and Microengineering, 2010.
67. Wang, Y., *Systematic prevention of bubble formation and accumulation for long-term culture of pancreatic islet cells in microfluidic device*. Biomed Microdevices, 2012.
68. Tang, L., *A facile route for irreversible bonding of plastic-PDMS hybrid microdevices at room temperatures*. Lab on a Chip, 2009.

10. List of figures

Figure 1.: A. Schematic model of a human placenta and fetus. B. Cross-sectional view of the placenta illustrates the placental cotyledons. Each cotyledon consists of a stem chorionic villus and its branches. C. The maternal intervillous space is separated from the lumen of the fetal capillary by the maternal-fetal interface composed of the syncytiotrophoblast, basal lamina, and villous endothelial cells.

Figure 2.: Blood circulation of the placenta, showing the directions of blood flow from mother to the placenta and fetal blood flow from the placenta to fetus.

Figure 3.: Schematic representation of the human placental barrier. The placental barrier cells develop thousands of microvilli exposed to the maternal blood in the intervillous space and regulate material transfer between the maternal and fetal blood flow.

Figure 4.:(a) The fabrication method of the PDMS contains soft lithography, thermal bonding, and compression-molding. (b) ECM incubation: matrix molecules adsorb to chamber surfaces by rows or individual chambers. (c) Cell loading: cell suspension are introduced to rows, while chambers are isolated to limit and regulate cells. (d) Culture:channels are designed to avoid cross-chamber communication: flows over/under other flows. (e) Assay: cells with desired probes are labeled with solution entered the array from the entry or exit channels.

Figure 5.: (a) The device has eight uniform structure units, each of them are connected to the reservoir, placed in the center of the device. (b) Magnifier schematics of the single structure unit with an upstream concentration gradient generator (CGG) and downstream parallel cell culture chambers.

Figure 6.: Brief overview of label-free substrate integrated cell-based biosensors. Different optical, mechanical and electrochemical transducer techniques allow for detection of various forms of cellular responses, like changes in metabolism, internal cell structure and cell morphology.

Figure 7.:Quartz crystal microbalance and its applications

Figure 8.: Different commercially available biosensing devices. A, Electric Cell-substrate Impedance Sensing (ECIS) for real-time, label-free, impedance-based method to study the activities of cells grown in tissue culture. B, xCELLigence is used to monitor cell proliferation and viability. C, Bionas 2500 monitors physiological parameters of living cells and tissue slices. D, Cellkey is a functional cell-based assay technology with high sensitivity to measure endogenous receptor targets in whole live cells.

Figure 9.: Placenta-on-a-chip. A. The upper and lower channel of the device is separated by a vitrified collagen membrane. B. Endothelial cells and trophoblasts are co-cultured on each site of the membrane mimicking a placenta barrier.

Figure 10.: The microdevice was fabricated by soft-lithography technique. Microchannels were created by PDMS with a channel dimensions of 1mm (width) x 1.5 cm (length) x 135 μ m (height).

Figure 11.: Electrical model of the cell. The cytosol can be modeled by a capacity and a parallel resistance, due to the intracellular membranes such as nucleus and mitochondrion furthermore other protein complexes.

Figure 12.: Schematics of TEER transwell VoltOhmmeter. B, equivalent model of the cellular barrier.

Figure 13.: Working principle of the EVOM2 VoltOhmmeter. Placement of the electrode is a critical

point in order to make accurate measurements. Reproducibility of the measurements can be improved by positioning the longer tip so that it touches the bottom of the dish each time.

Figure 14.: Schematics draw of electrical impedance spectroscopy

Figure 15.: Neubauer chamber for cell counting, performed under the microscope.

Figure 16.: Channel design of the first microfluidic chip to carry out cell adhesion measurements.

Figure 17.: Assembled blank chip with adhesive tape and polymer tubes to ensure microfluidic flow for cell adhesion measurement.

Figure 23.: AutoCaD design of the electrodes and microfluidic channel. A, each chip consisted of seven sensors in order to carry out parallel measurements. B, additional AutoCad design was made for each sensor to ensure a well defined microfluidic channel for the cells.

Figure 18.: Final chip design for electrical impedance measurement. This PDMS thickness (3 mm) was not suitable for the cutter; therefore the channels were cut out by hand, using a standard, in order to get equal size.

Figure 19.: Placenta station with syringe pump (A), degaser (B), waste (C), chip fixed by springs and screws (D) and valves (E) to ensure a bubble-free injection of the cells .

Figure 20.: Different cell lines cultivated in 48 transwells. Seeding density was 25000 cells/well. After 24 h seeding, the cells are attached on the surface and started to proliferate.

Figure 21.: Cell viability after 4 hours of colchicines exposure.

Figure 22.: Cell viability after 4 hours of MMS exposure.

Figure 23.: Cell viability after 4 hours of chlorpromazine exposure.

Figure 24.: B30 cell viability after exposure of toxins with different concentrations.

Figure 25.: ATCC cell viability after exposure of toxins with different concentrations.

Figure 26.: B30 cell viability after 4 hours of exposure of SiO₂.

Figure 27.: ATCC cell viability after 4 hours of exposure of SiO₂

Figure 28.: TEER measurement without and with PBS wash.

Figure 29.: TEER measurement with five placenta cell line with the seeding density of 10⁵ (A), 5*10⁴ (B) and 2.5*10⁴ (C).

Figure 30.: The effect of colchicines, MMS and chlorpromazine on ATCC and B30 with different seeding densities: A. ATCC 10^5 cells/well, B. B30 10^5 cells/well, C. ATCC $5 \cdot 10^4$ cells/well, D. B30 $5 \cdot 10^4$ cells/well, E. ATCC $2.5 \cdot 10^4$ cells/well, F B30 $2.5 \cdot 10^4$ cells/well.

Figure 31.: B30 TEER measurement after 4 hours of SiO_2 exposure

Figure 32.: ATCC TEER measurement after 4 hours of SiO_2 exposure

Figure 33.: Cell adhesion mechanism

Figure 34.: Air bubble formation over the time with the different chip design.

Figure 35.: Not suitable period of time and power of plasma exposure lead to delamination of the electrode.

Figure 36.: Grading: 5: very good adhesion, 1: very bad adhesion

Figure 37: The conductivity of the applied PBS concentrations can be seen on figure a. Figure b shows the impedance of the solutions with increasing concentrations

Figure 38.: After cell adhesion, the effect of an air bubble can be observed. In the case of $4 \mu\text{l}/\text{min}$ flow rate, the air caused cell death, as the impedance decreased to the initial value.

Figure 39.: Real-time impedance measurement of B30 cells. After 24 hours, MMS was introduced to the channel.

Figure 40.: Electrode delamination due to chlorpromazine. This issue not only resulted in a failure of impedance measurement but also lead to cell death.